Systematic Oxidation of Bi_2O_2Se Semiconductors with Metal Oxide Layers

by

Sushin Dahal

A Thesis Presented in Partial Fulfillment
of the Requirements for the Degree
Master of Material Science

Approved April 2026 by the
Graduate Supervisory Committee:

Seth Ariel Tongay, Chair
Sui Yang
Yang Jiao

ARIZONA STATE UNIVERSITY

May 2026

ABSTRACT

Bismuth oxyselenide (Bi_2O_2Se) has emerged as a promising layered semiconductor due to the high carrier mobility, stability, and potential for its integration into next generation electronic devices. However, the manufacturing processing for this material remains incomplete. Particularly, the forces governing oxidating and phase transformation. Understanding these mechanisms is essential for developing reliable synthesis strategies.

In this work, the systematic oxidation of bismuth selenium and bismuth oxy-selenide thin films were studied with controlled oxygen reservoir and oxygen scavengers. The oxygen reservoir material was hafnium oxide (HfO_2), which was placed on bismuth selenide (Bi_2Se_3) to oxidize into Bi_2O_2Se. The oxygen receiver was a titanium (Ti) capping layer on Bi_2O_2Se to allow phase transformation into Bi_2Se_3. These materials were annealed at various temperatures in a controlled environment to study the oxidation reaction and the driving forces behind them.

Thin films of Bi_2Se_3 and Bi_2O_2Se were synthesized by chemical vapor deposition (CVD) and pulsed laser deposition (PLD). The capping layers were deposited with atomic layer deposition (ALD) and sputtering.

Results show successful oxidation and scavenging with the metal oxide layers as nickel oxide (NiO), Titanium (Ti) and hafnium oxide was utilized (HfO_2)

ACKNOWLEDGMENTS

My committee, Dr. Sui Yang, Dr. Yung Jaio, and my PI, Dr. Seth Tongay. My colleges, Angela Caroliny Agra Pinto, Cauê Nogueira, Melike Erdi, Ethan Swonger, Patrick Hays, Owyn Colwell, Dohee Kim, Dinushika Vithanage, Aixin Zhang, Renee Sailus, Caiti Downs, Cheng-Lun Wu, Dohee Kim, Blake Povilus, and Yunbo Ou. Family, my parents and my sibling. My partner, Andy Dao. Lastly, my friends who have helped me through this process.

TABLE OF CONTENTS

Page

LIST OF TABLES

LIST OF FIGURES

CHAPTER 1, INTRODUCTION

1.1 Background and Motivation

The current semiconductor architects utilize silicon (Si) and silicon dioxide (SiO2). Over 95% of electronics dependent on this material system (Y-J.2024) . However, the future of electronics is running into the limits of Moore's law (Saurabh, 2025). Before the issue dawns upon the semiconductor industry and leaves it with no viable options, the exploration of alternatives for the future of electronics must be explored.

The next generation of electron, magnetic and optical technologies has quite a few viable options including Bi_2O_2Se two-dimensional (2D) materials, gallium nitride (GaN), silicon carbide (SiC), and quantum dots (Dull 2024). For these options, the viability of quantum dots is not apparent with the current architecture not reaching such scales yet. SiC and GaN are high bandgap semiconductors where most architecture is made for materials closer to silicon's bandgap[1]. With this, Bi_2O_2Se and 2D materials can be explored with a more in-depth lens.

1.1.1 Two-Dimensional Materials

2D materials are enabled by mechanical exfoliation, which was a major breakthrough in the field as early as 2004[2]. The bottleneck with this material is that mechanical exfoliation by tape is not scalable or reliable manufacturing. Other 2D material options have come about, which are 2D MXenes, transition metal dichalcogenides (TMDCs), and Moire nanostructures. Most 2D materials have strong in plane covalent bonds while the interlayer forces are weak Vander Waals interactions.[3] the ability to

exfoliate such materials and maintain stability is a great discovery. With that, the first 2D material that will be explored is MXenes.

MXenes have a diverse structure due to the diversity in elements that can constitute it. The general formula is M(n+1)X(n)T(x), where M is an early transition metal, X can be carbon or nitrogen, and T(x) is for the surface termations[4]. The elemental diversity allows a mix-and match structure for the properties desired, as they have large exposed surface area, high electronic conductivity, strong mechanical properties, high ionic conductivity, and hydrophilic behavior[4]. Processing for these materials includes the use of hydrogen fluoride (HF), HCl-hydrothermal etching, halogen etching, and Lewis acidic molten salts[4]. Due to the nature of the wet chemistry and dangers that do not integrate with the current semiconductor processing industry, there might be difficulties with MXenes within the current semiconductor environment without major overhaul.

TMDCs can be produced by pulsed laser deposition (PLD), atomic layer deposition (ALD), molecular beam epitaxy (MBE), and chemical vapor deposition (CVD)[4]. CVD production has been the most studied but oftentimes has uncontrolled reactions with chalcogens leading to poor crystallinity. To address this, metal-organic CVD (MOCVD) has shown better results due to increased control over the supply the precursor[4]. The issues can be grouped into three main categories for mass acceptance of TMDCs and their commercialization. Lack of defect control along the grain boundaries leading to antistites, vacancies, and interstitials make it difficult to adopt[4]. The lack of a clean surface, with dangling bonds that are reactive to the atmosphere makes the material lack the stability required of it. Lastly, there is a lack of dopant uniformity with the production[4] is clearly an identified issue.

Moire nanostructures and systems are when two 2D materials are layered on top of one another and create a surface where the electronic wavefunctions strongly overlap. Strong electronic wavefunctions overlap when the 2D materials are stacked in such a way that the van der Waals crystals have a lattice mismatch, or relative twist angle. When the Moire pattern arises, there is a tunable superlattice that can lead to an inherently altered Berry curvature[5,6]. Berry curvature leads to nontrivial topology and quantum geometry. Moire lattices are a promising endeavor; however, there are challenges in progressing them. There are some extreme fabrication challenges that are related to the inherent material needing the precise angle between the two materials, lack of thermal stability, difficult at scale, and clean room requirements[4].

1.1.2 Bismuth Oxyselenide as a Candidate

The last material as a viable Si replacement or material to work in conjunction with Si, is Bi_2O_2Se. Bi_2O_2Se is not a 2D material, although it is a quasi-2D layered material with a zipper-like layered structure. According to Ding in 2022, the material crystalizes into a "layered body-center tetragonal structure (a=b=3.887 A, c=12.164 A)[7]. Previous studies have demonstrated that Bi_2O_2Se has high carrier mobility[7], air stability, and strong potential for new devices[8]. Figure 1 shows the atomic structure of Bi_2O_2Se.

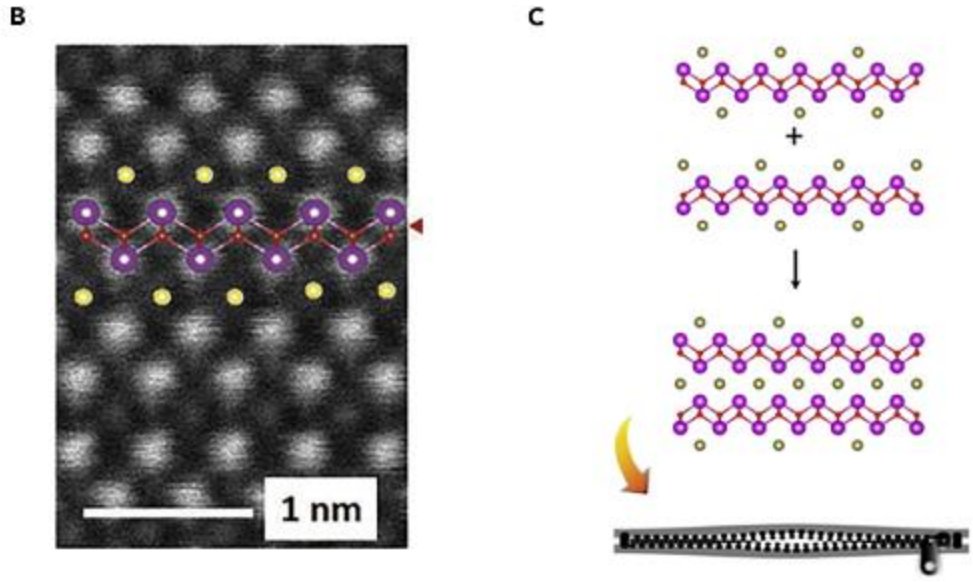

Figure 1 sources from Deng et all[9]. This shows the tetragonal structure of Bi_2O_2Se. It also shows the proposed 2D zipper model for Bi_2O_2Se when there is a bilayer.

Whereas, the benefits are plentiful, a bottleneck arises. The controlled synthesis and processing of Bi_2O_2Se remains challenging. More specifically, the oxidation interactions with bismuth-selenium compounds are not fully understood. To create a controlled fabrication of Bi_2O_2Se there needs to be a better understanding of the basic oxidation issue and influence.

To gain information, a promising approach is to control the oxidation of Bi_2Se_3 thin films. Oxygen can be introduced through external oxide layers. Oxygen can also be removed through annealing with external oxide scavengers. This can enable phase change from Bi_2O_2Se to Bi_2Se_3, with the external metal layers acting as an oxygen scavenger (Titanium) or donator (HfO_2). This will enable phase transformations under controlled thermal conditions. This behavior is largely unexplored with Bi_2O_2Se.

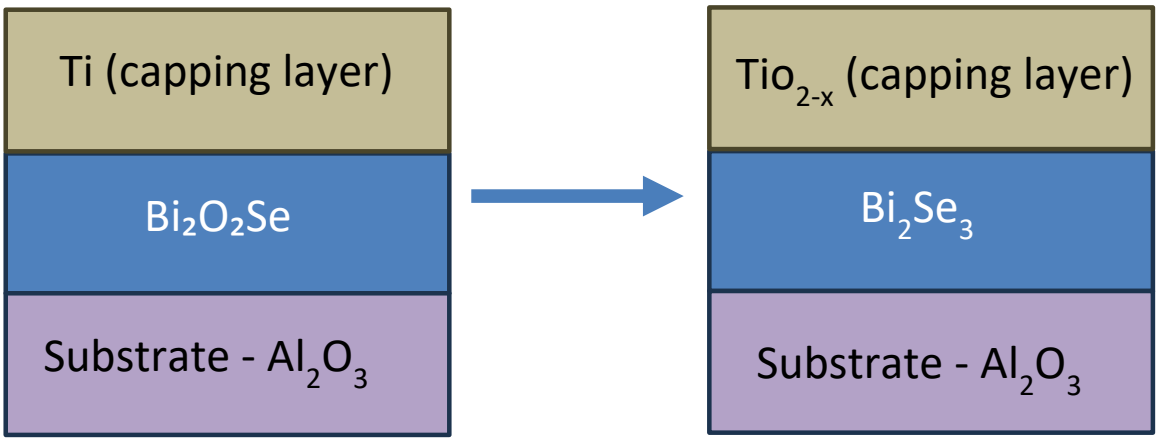

Figure 2. shows the concept behind this mechanism. Systematic and controlled oxidation through limited oxygen sources and scavengers will allow phase transformation, which will explain the processes for more controlled synthesis paths for the future.

1.2 Research Gaps and Objectives

There is currently a limited understanding of how a limited oxygen reservoir can affect the oxidation of Bi_2O_2Se. As well as the effects it will have on the stress line with this oxidation process. Another limited understanding of how sputtered metal film quality influences the conversion process and the resulting crystallinity and uniformity of layered compounds.

Objectives of this work include:

•Establishing a controlled oxidation route for the material through metal oxides being used as an oxygen reservoir

•Studying the phase changes that are acquired with oxidation and annealing

•Demonstrating CVD oxidation on these materials.

1.3 Thesis Organization

This thesis is organized into five chapters. Chapter 1 provides the background, motivation and research objectives. Chapter 2 reviews the literature on the material system, synthesis methods, and characterization related to this work. Chapter 3 presentes the experimental methods and growth configurations that were used in this study. Chapter 4 presents the Bi_2O_2Se oxidation and annealing results. Chapter 5 concludes the work and outlines future research.

CHAPTER 2

LITERATURE ON MATERIAL SYSTEMS AND SYNTHESIS METHODS

2.1 Overview of Target Material Systems

Bi_2O_2Se is a high mobility semiconductor with compatibility for thin-film device architecture. Properties from this Bi_2O_2Se garner a great deal of interest and applications for next generation of electronic and optoelectronic devices. Bi_2O_2Se has a high carrier mobility around 28,900 cm2 V^{-1} $s^{-}1$ at 1.9 K and about 450 cm2 V^{-1} s^{-1} at room temperature[9]. As well as an indirect bandgap that starts at 1.9eV with just the monolayer.[10] In bulk the bandgap is ~0.8eV[10].

Another highlight of this material is air stability compared to other 2D materials, layered structure, and compatibility with oxide interfaces. Bi_2O_2Se has natural oxide formation that led to Bi2O5Se layers[9] that are like traditional Si/SiO2 interfaces currently in semiconductor technology. However, a major difference is SiO2 oxide layer is amorphous while the oxide layer for Bi_2O_2Se is a crystalline structure[9]. The crystalline nature of the layer allows for less defects and disorder due to the nature of being in the *Abm2* space group[9]. Other properties that highlight this material is the high crystallographic symmetry, strong spin-orbit coupling, and excellent environmental stability[9]. Band structure engineering can also be done with Bi_2O_2Se with stress and strain changing the electrical, magnetic and optical properties. Band structure engineering can be tunned with thickness variations, in-plane biaxial strain, and surface defects[8]. The surface defects are due to oxygen absorption on selenium vacancies when there are freshly cleaves Bi_2O_2Se surfaces. This exposure leads to a reduction in the conduction band electron filling, which may regulate the carrier concentration[9]

Growth of Bi_2O_2Se varies due to the multiple synthesis options that can be utilized, chemical vapor transport (CVT), molecular beam epitaxy (MBE), chemical vapor deposition (CVD), pulsed laser deposition (PLD), and hydrothermal synthesis.[9] This paper will highlight CVD and PLD for Bi_2O_2Se.

Bi_2O_2Se had garnered a great deal of interest for applications in field effect transistors, photo detectors, and various other next generation electronic devices. Although not a traditional van der Waals system, it displays low dimensional electronic behavior. Control of phase formation, from Bi_2Se_3, and crystalline remains a challenge.

2.2 Overview of Target Material Systems and 2D materials

This work focuses on the thin film Bi_2O_2Se and Bi_2Se_3 designed to control oxygen transport and phase change at high temperatures. This is done with limited oxygen reservoirs and oxygen accumulation layers. The configurations that are utilized in this paper are highlighted below.

Growth Method	Deposited material	Substrate	Capping layer
PLD	Bi_2Se_3	Si	HfO_2
PLD	Bi_2O_2Se	Al2O3	Ti
CVD	Bi_2Se_3	Si	HfO_2
Sputtering	Bi_2Se_3	Al2O3	NiO

Table 1. Material systems and capping layer configurations used in this study

In these materials, there is either an Al2O3 or Si substrate where a Bi_2Se_3 thin film is deposited on top. Then there is another thin film of either HfO_2 acting as an oxygen

reservoir or Ti acting as an oxygen acceptor. The hypothesized role of HfO_2 is to supply oxygen to the material so that Bi_2Se_3 can transition to Bi_2O_2Se. As for the transition metal Ti, it may act as an oxygen sink to remove oxygen from the surrounding layers so that Bi_2O_2Se can transition to a material with less oxide or even back to Bi_2Se_3.

With careful engineering of the structure and layers – the oxygen movement between the layers. This will warrant more information into the interactions of Bi_2O_2Se with a reservoir to see the reactions. Since this is an uncharted area of knowledge this will give insight to see if the oxidation behavior differs from traditional oxidation processes where the oxygen is abundant.

2.3 Synthesis Methods.

In this work, Chemical vapor deposition (CVD), pulsed laser deposition (PLD), atomic layer deposition (ALD), and sputtering are the main deposition methods. Each technique serves a different role in the fabrication of the layered thin film stacks.

2.3.1 Chemical Vapor Deposition for BisSe3 Growth

Chemical vapor deposition (CVD) is a versatile synthesis process where the atomistic vapor-transport process is utilized[11]. The general process of CVD involves forced flow, adsorption, chemical reaction, and diffusion out. This is happening in a closed environment with a quartz tube and a CVD furnace as a heating element. There is a vacuum pump to control the environment inside the quartz tube. Lastly, there are lines to flow gases into the controlled environment. The precursors are placed at certain temperatures while

the substrates are down the line at another temperature range. To understand these concepts more, it's best to start with the definition of atmospheric vapor transport.

Figure 3. And a quick schematic. And explain the system. Type of equipment, homemade build, etc.

[11]Atomospheric vapor transport is a synthesis method where the building blocks of a material are individual atoms, molecules, or atoms and molecules transported through a vapor phase. This category includes CVD, and physical vapor deposition (PVD). This is the general CVD process[11].

The first stage is forced flow where the reactant gases are flowed into the reactor chamber, and the gas flow must interact with the heated substrate. Around the substrate there is a region of slow-moving gas near the surface called the boundary layer[11]. This is defined through fluid dynamics. The higher the pressure, the slower the laminar flow. This

reacts in the reactions diffusing through this layer to reach the substrate[11]. The thickness of this boundary layer is inversely proportional the Reynold's number.

$$Re_x = \frac{\rho u x}{\mu}$$

$$\Delta = \frac{x}{\sqrt{Re_x}}$$

Here, the Reynolds number is a dimensionless parameter that characterizes the flow of fluid, where gas flow is assumed to be generally laminar[11]. To define Re_x, there is mass density, ρ, times the flow velocity, *u,* multiplied by the distance of the inlet flow of the tube *x*. The Δ is the thickness of the boundary layer. Δ is defined by *x*, over the square root of Re_x.

Afterwards there are surface kinetics and Adatoms. This process is apparent during the formation of solid films. This defines the adatom movement when it resides at an adsorption site on a 2D lattice and then moving across these adsorption sites, where the adatom will make multiple jump attempts and multiple sites[11]. This is first determined by the mean residence time for the adatoms, defined by τ_s below[11,12].

$$\tau_s = \tau_v \exp\left(\frac{E_{ad}}{kT}\right)$$

τ_v is the period of the vibration that is perpendicular to the surface. E_{ad} is the adsorption energy of the adatoms on the substrates over kT. k_b *or* k is the Boltzmann constant, times the temperature[13]. The diffusion depends on the potential energy barrier. This barrier can decide the diffusion rate from the material that will be deposited onto and the chemical itself. This equation allows us to define the thermal equilibrium of the

adatoms, τ_e where one can see how long the adatoms will stay on the substrate and understand how the thin film will be created[12]

$$\tau_e = \tau_s \exp\left(\frac{-E_{ad}}{kT}\right)$$

The time limit is the mean surface time is dependent on the relationship of E_{ad} to kT. If the $E_{ad} >> kT$, there will be attachment onto the surface[11,12]. If the $E_{ad} \sim kT$, there is re-evaporation. While it would be ideal for the adatom to continuously move throughout the sample to react, there is limited time for this reaction until there needs to be re-evaporation.

If the adatoms stay on the surface, the attempt frequency is simplified to be the vibrational frequency of the adatom to see how many times it will jump which is the Brownian movement for the continuous random movement. The traveling time for the diffusion on the surface is defined by, τ_d [12].

$$\tau_d = \tau_p \exp\left(\frac{E_d}{kT}\right)$$

τ_p is the lattice period of the thermal vibration parrllel to the surface. E_d is the surface diffusion energy of the adatoms against the potential energy barrier of the substrate surface[12]. Then the mean travel time of the adatoms, *X*, is defined by.

$$X = \sqrt{2 D_s \tau_s}$$

$$D_s = a_o^2 / \tau_d$$

$$X = a_o \exp\left[(E_{ad} - E_d)/2kT\right]$$

a_o is the lattice spacing of the surface atoms. The diffusion of the adatoms strongly depends on the E_{ad} *and* E_d [12]. The surface mobility of adatoms defines the quantity and

the structure of the deposited film from gran size, surface smoothness, and epitaxial growth[11,12,14].

Once the adatoms touch down onto the surface, there are multiple ways for the adatoms to diffuse across the surface for the film formation. The formation of films falls into three categories. There is Volmer-Weber (island growth), where small clusters form and grow into 3D islands. Frank-van der Merwe (Layer growth) where the atoms attach to surface states with preferential orientation resulting in continuous growth of 2D layers. Lastly there is Stranski-Krasnov (Mixed Growth) that is simply a combination. Growth starts as layers and then turns to island growth[11,15].

The last step to the atomistic vapor transfer process in CVD is tahr the chemical reaction near the heated surface involves the disruption of the gaseous by-products. Desorption of the byproducts diffuse out through the boundary layer. While CVD and PVD are similar, PVD at this step is generated through the simple condensation of the solid form into the substrate.

The quality of the deposition depends on the surface mobility of the Adatoms. The adatoms in this process can diffuse with multiple methods, hopping, atomic exchange, tunneling diffusion, vacancy diffusion. There is hopping or jumping where this is the most common and basic. There is a meta stable transition between the adsorption sites to allow the Adatom to temporarily reside. Γ is the frequency of the moevemnt.

$$\Gamma = \nu^{-E_{diff}/k_B T}$$

The attempt frequency is, v, $-E_{diff}$ is the potential energy barrier.[14]

Atomic exchange is the next method. The adatom and adjacent atom exchange within the surface lattice. The displaced atom becomes adatom. this happens in hertodiffusion systems[14]. There are still some of the basics that need clear understanding. Tunneling diffusion is quantum tunneling effect in the material. Particles tunnel across the diffusion barriers where there is a case of a low diffusing particle mass and a low potential energy for diffusion[14]. Rates are temperature dependent. Lastly is the vacancy diffusion, which is the most common method of surface diffusion at high coverage levels. Observance of this is difficult currently due to high diffusion rate and low vacancy concentration[14].

Another deciding factor for film quality is substrate temperature, deposition rate, kinetic energy of the incident species, and the temperature of the precursors. Gaining more epitaxial growth is depends on the high substrate temperatures so that the deposited film mimics the substrate's crystal structure[14].

2.3.1.1 CVD of Bi_2O_2Se

There are works where Bi_2Se_3 was grown in CVD, such as Liu et al with CVD[16]. Other works are.

The Bi_2Se_3 deposition was a biproduct of attempting Bi_2O_2Se synthesis in CVD, but other works have helped us to adapt and create Bi_2Se_3 thin films, such as above. This work utilized low pressure CVD where Bi_2Se_3 powder was placed inside a ceramic boat of a CVD furnace and then Argon was flowed. The growth temperature was 630 on the furnace and the method of cooling was quenching with a fan.

The original growth of Bi_2O_2Se film in CVD was based on other works such as Sagar et al[17], and reviewed in Lee's paper as well[18]. The reason Bi_2O_2Se was not grown in

CVD was due to the thickness of the thin film exceeding the thickness limits of 50nm. Due to this, the process to produce thin Bi_2O_2Se was designated to be PLD.

2.3.2 Pulsed Laser Deposition

Pulsed laser deposition is a versatile deposition tool for depositing any material and allows the material to maintain stoichiometry. This is a great tool for creating materials that are complex and high temperature semiconductors that require precise processing. The general process is a high intensity laser beam focused onto a target material inside a vacuum change. The focused laser beams with create a plume and then deposits onto the surface of the substrate.

The process can create thin films with these main components a powerful laser, a source material, high vacuum chamber, and a substrate holder. The laser is an excimer laser which emits high energy ultraviolet light to vaporize the target material. The laser has an oscillator to generate laser pulses, optical amplifiers for tuning pulse energy. Then to control the pulse shape, wavelength, and beam focus. Wavelength of the beam needs careful selection depending on the material to be ablated[15].

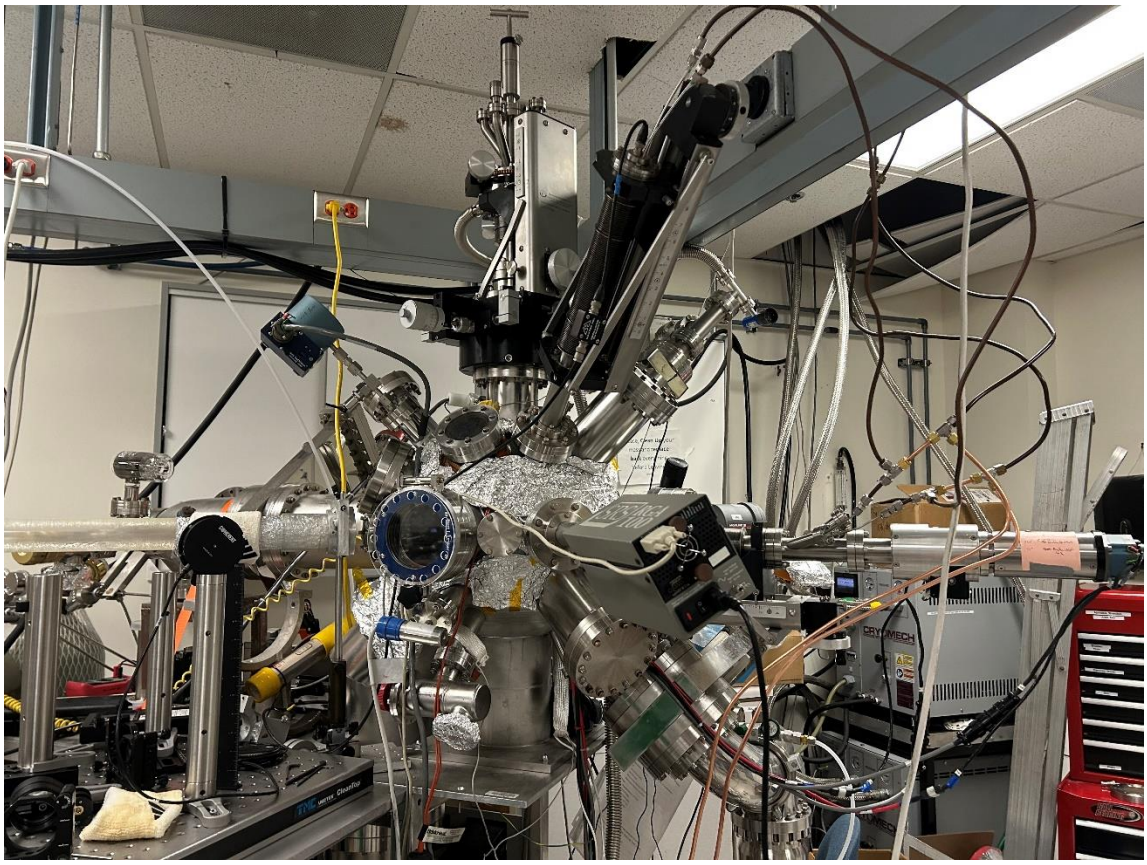

Figure 4. the PLD system utilized.

Within the chamber, the target material carousel (also called a platen), there is secure course for the target material and control of its movement. This carousel controls the movement of the material during the ablation process by continuously rotating the target. Rotation of the target is vital to prevent "trenching"[15]. Trenching occurs when the laser strikes the same spot repeatedly and creates a crater or trench into the material. This can be a problem later since it changes the ejection angle of the plasma plume and the laser fluence during impact. This can negatively affect the film's growth and thickness uniformity. Ensuring the lack of trenching happens through target rotation – allowing an

even raster of the target. This is also a cost-effective approach so that the target can be used more. The carousels in high power systems have a water cooling to keep the target cool[15].

The high vacuum chamber is made up of stainless steel or quartz tube chamber. high vacuum chambers are heavy duty in preventing contamination. With the high vacuum, and the chamber the purity of the deposition is ensured. The low pressure allows for the material deposition energy density to be high and have an efficient deposition, especially regarding the plasma plume. These high vacuums enable the stoichiometric cohesiveness for the target material transfer to the substrate. The chemistry in the plum is gained through keeping a high mean free path with unimpeded travel. Thus, allowing vaporized atoms to travel more uniformly from the source in the plasma plume. Within the plume as well, there needs to be minimal material collision so that the materials do not slow down or react too early[15].

Lastly, there is the substrate holder. The distance of the holder in relation to the target, temperature measurement, rotation, and process control all depend on the substrate holder. After laser ablation in PLD, there is forward directed plume of material, so the substrate holder must be directly opposite of the target. Regarding this, the target carousel to substrate holder distance is vital as it depends on the energy of the material during the deposition time. The thermals of PLD matter as they are critical to allow proper adhesion and crystallinity to the substrates. In the previous section (2.3.2), the temperature of the substrate matters for the adatoms on the material, which applies here. The heating method requires careful attention as there might be resistive heaters, quartz lamps, or even CO2 lasers for a direct radiative heater. To ensure film uniformity, across the narrow angular distribution of the laser plume, the holder needs to rotate the substrate so that the variation

of the plume's thickness and composition can be averaged out. For the last role that the sample holder can take on is as a process control or diagnostics control[15]. Mounting points can be present on the holder so that it can accommodate thermocouple or allow pyrometers to measure the temperatures and the surface temperature[15].

For the PLD process, there is laser pulse interaction, plasma formation, material ablation, debris removal, and surface modification[15]. The laser pulses to the target surface which ethe laser pulse energy is absorbed by the material causing rapid heating and thermal excitation. As the temperature and electron density increase, the material undergoes ionization. The ionization of the material results in a plasma plume.

These two steps happen in the first few nanoseconds from the high energy of the laser creating a high-pressure bubble of hot plasma on the target surface (pressure as high as 10 to 500atm[15]). This plasma consists of atoms, molecules, ions, and electrons. There are certain conditions in which clusters or particulates may be present. The species possess very high kinetic energies that are called super thermal energies where the ions have transitional energies ranging from 40 to 70 eV[15]. The reaction continues to the plume itself. There is the Knudsen Layer (KL) that is very close to the target surface where the particles collide frequently reaching a local equilibrium since the species are thermalized. Then the plume moves away from the target with a velocity distribution called a shifted Maxwellian[15]. The plume expansion and movement can be define by gas dynamics laws related to this shifted Maxwellian velocity distribution[15].

$$f(v_x, v_y, v_z) = \frac{n_K}{\left(\frac{2\pi k_B T_K}{m}\right)^{3/2}} \frac{E_j^{\frac{j}{2}-1}}{\Gamma\left(\frac{j}{2}\right)(k_b T_k)^{\frac{j}{2}}} \exp\left[-\frac{2E_j + m\{(v_x - u_K)^2 + v_y^2 + v_z^2\}}{2k_b T_K}\right]$$

n_K is the number density near the Knudsen layer boundary and T_K is the temperature near this boundary[15]. u_K is the flow velocity where the outer boundary is equal to the local speed of sound in the chamber[15]. E_j is internal energy and j is the internal degrees of freedom of escaping particles. v_x, v_y, v_z are the respective velocities in those respective, x, y, z directions[15].

Expansion dynamics and internal collision result in a forward directed plume toward the substrate. When there is gas flowing into this chamber, there can be attenuation affects where the plume species slow down with collisions if it is a non-reactive gas. With reactive gas, there will be new compounds such as oxides deposited onto the surface. Instantaneous deposition rate happens due to the speed and high energy of the process[15].

The deposition of the material follows nucleation theory where the formation of new phases forms a metastable stare are created. The substrate to growth type can be described below[15], as mentioned earlier in the paper.

$$X = a_o \exp\left[(E_{ad} - E_d)/2kT\right]$$

As for film growth method or outcome, this is governed by the surface energies of the adatoms, called the wetting factor[15]. This is dependent on the difference in surface energy γ_s of the substrate to the film γ_f to give the interfacial energy γ_{fs}. Layer growth occurs when $\gamma_s - \gamma_{fs} > \gamma_f$[15].

For this study, two materials on two substrates were deposited by PLD by a lab mate, Angela, Agra Pinto. Bi_2O_2Se films were deposited onto Al2O3 and Bi_2Se_3 films were deposited onto Si substrates for this work.

2.3.3 ALD

Atomic layer deposition (ALD) is vapor phase thin film deposition technique. The vapor phase allows for precise thin film control and composition. This is a self-limiting process. ALD is like CVD but differs in the precursors and cycles of heating.

ALD has repeated cycles with two precursor chemicals. The first step exposes the substrate to a gases precursor that reacts with eh active sites on the surface[19]. This is the chemisorbed layer that will saturate the surface. Excess precursor is removed buy purging the chamber with an inert gas, such as Argon[19]. The second cycle a second precursor is introduced and reacts with the chemisorbed layer to release violate by products[19]. Another purge cycle happens for this material as well[19]. These cycles are repeated to gradually build the film with atomic scale thickness control[19].

ALD is sued for the deposition of high-quality dielectrics[19]. In this work, one of those materials is Hafnium Dioxide. Material plays an important role in the semiconductor industry. ALD deposited HfO_2 layers are controlled oxygen reservoir to promote the phase change of the Bi_2Se_3 thin film stacks. The controlled growth of HfO_2 allows for a certain thickness of oxide within this reservoir.

2.3.4 Sputtering

Sputtering is a physics vapor deposition technique that involves the physical ejection of the atom form a source material (the target) onto a surface (the substrate) to form a thin film. The process is exothermic as it relies on the momentum and transfer of

energetic ions[12]. The sputtering process occurs in a high vacuum so make sure there is a clean path while the target is ionized. The steps in this process are ionization, plasma formation, bombardment, and deposition.

The ionization step happens after the sputtering chamber is put under vacuum and refill with an inert gas. This gas is commonly Argon[12]. The operating pressure is dependent on the system and the sample[12]. While a plume is utilized for deposition, there is a difference from PLD. Where a high voltage is applied to the target create a discharge of plasma[12]. The target is a cathode to make sure this process is possible. Afterwards, the accelerated inert gas ions strike the target material to knock the atoms from the target surface[12]. Many Argon atoms are hitting the target repeatedly to eject atoms. The deposition happens when the ejected atoms move across the vacuum chamber and condense on the substate to from the film[12].

2.4 Characterization Techniques

2.4.1 X-ray Diffraction (XRD)

X-ray diffraction (XRD) is a characterizing tool for thin films. This can be utilized for 2theta/omega scans, grazing-incidence scans, rocking curves, pole figures, and azimuth scans. In this work, this and this will be utilized[20].

XRD is a non-destructive characterization tool which gains information about film composition, film thickness, degree of crystallinity, and the density of the dislocations.

The instrument is composed of an x-ray source, detector, incident optics, receiving optics, and the goniometer[20]. The source produces x-rays with a variety of options, x-ray tube, rotation anode x-ray generator, microfocus time, and a synchrotron[20]. The facility where the study was done used the smart lab Rigaku XRD (Copyright, Smart Lab)[21,21] This

tool utilized a rotating anode X-ray generator[20]. The target is a rotating cylinder that is water cooled on the inside to cool down the focal spot. Traditional x-ray sources, such as the x-ray tube, produce high temperatures since the tungsten filament is heated by an electric current with a high voltage so that electrons can accelerate. These electrons hit the anode to excite the x-ray photons. X-rays come from K alpha radiation. There are signs of K_{beta}but those are either removed by a Ni filter or a monochromator[20].

The detector converts the X-ray into an electrical signal. The signal is usually. This information is obtained through the elastic scattering of the X-rays on the atomic planes. These x-rays have a wavelength, lambda, that is in the order of nanometers which allow the x-rays to interact with materials and scatter or have an interference pattern resulting from the material's atomic planes[20].

This can be modeled by Bragg's Law, $n\lambda = 2d_{hkl}sin\theta_B$. The Bragg equation can be defined as θ_B is the Bragg angle, the Miller indices of the crystal plane are d, and the subscript hkl denotes the interplanar spacing. This is equal to n, which is the integer to reference the diffraction maxima, and the λ is the wavelength of the X-ray beam[20].

The x-ray will then scatter depending on the planes at angle theta, which is the same as the incident angle in relation to the crystalline plane. By analyzing the diffraction pattern, the crystalline phase, grain size, and texture can be measured[20].

2.4.2 Scanning Electron Microscopy (SEM)

Scanning electron microscopy (SEM) is a nondestructive characterization technique for surface analysis, crystalline structure, and chemical composition. The SEM is made up of the electron source (gun), condenser lenses, objective lenses, X-Y scan soils, scan generator, detectors, sample stage, and external vacuum pumps[22–24]. The electron

source has a focused beam of high energy electrons that scan across the surface of a specimen[22,23]. The vacuum within the SEM column ensures that the electron beam travels easily to the sample without scattering by other means[22,23].

This electron source can be a tungsten (W) filament, lanthanum hexaboride (LAB6), cerium hexaboride (CEB6), or field emission gun (FEG)[22,23]. For the tungsten filament, there is our V shaped wire of W, which is heated resistively to produce electrons. This operates at high temperatures[24]. As for LaB6 or CeB6, they work in similar manners[24]. These materials have a sharp tip in allowance for thermionic emission. Hexaboride crystals allow for a high beam current at lower cathode temperatures compared to that of tungsten. Lastly there is a field emission gun (FEG) source[24]. This is the source that was utilized in this work. The FEG source is a wire of W with a less than 100nm sharp tip[24]. The process to create the beam is the field election emission. The FEG source is a Schottky FEG where they function as field-assisted thermionic emitters - thus when the electric field is applied to the tip to extract the electrons and a second field is used to accelerate then down the column[24].

The lenses are electromagnetic lenses to manipulate the electron beam in SEM. The applied magnetic field of the solenoid copper wire is dependent on the strength of the current passing through[22,23]. This magnetic field affects the off-axis electrons path toward the optic axis to in turn have a beam crossover at a specified distance from the lens. The condenser lens reduces the diameter of the primary beam from the electron source down the column. The objective lens is the final lens to focus the beam onto the sample surface by establishing the working distance and probe size[22,23]. Scanning coils are after the beam

is focused. The purpose of the scanning coils is to deflect the beam in relation to the X and Y axes so it can affect the rastering over the surface[22,23].

With the column defined, there is the sample chamber where the samples are mounted and kept under vacuum. After the electron beam interacts with the sample in SEM, there are detectors to distinguish secondary electrons, backscattered electrons, or characteristic x-rays. For each electron energy there are detectors for this[22,23].

When the electrons beam interacts with the sample, it hits the atoms within the sample. Electron to sample interaction results in elastic scattering of the electrons[22,23], backscattered electrons; and inelastic scattering of the electrons, secondary electrons[22,23]. Lastly, there are characteristic x-rays.

Back scattered electrons (BSE) provide the composition contrast due to their high energy interactions between the beam and the sample that are nanometers in depth[22,23]. These electrons interact with the atomic nuclei of the sample due to columbo interactions causing large angle scattering[22,23]. This is elastic scattering due to the minimal energy loss during this interaction, allowing for more of a compositional contrast that is proportional to the atomic number, Z[22,23]. When the heavier element appears brighter in BSE images. Thus, this is where phase identification comes into play[22,23].

The BSE detector is composed of several semiconductors located around the bore of the microscopes final lens to detect high energy elastically scattered electrons[22,23].

Secondary electrons [SEs] have lower energy than backscattered electrons due to the nature of their inelastic scattering of the primary electron beams. The depth of the electrons is only 5-10nm[22,23] of the sample allowing surface imaging and topography.

To detect secondary electrons with inelastic scattering, there is the Everhart-Thornley detector that utilizes a phosphorates coated scintillator in a faraday cage to attract secondary electrons[22,23]. The scintillator is a material that emits photons in the ultra-violet region of the electromagnetic spectrum when it absorbs energy from gamma rays[22,23]. With this absorption, there is a change of the absorbed energy into electric signals[22,23].

In this work, SEM was used to examine the morphology and cross-sectional structure of thin films before and after annealing. Cross sectional SEM was particularly useful for evaluating interfacial diffusion, structural changes from the oxidation process, and some thin film thickness evaluation.

2.4.3 Energy Dispersive X-ray Spectroscopy (EDS)

Energy Dispersive X-ray Spectroscopy (EDS) is an analytical technique used in conjunction to SEM to determine the elemental composition of materials. Earlier, characteristic x-rays from the previous section were mentioned, and will be defined in this section.

When the electron beam ionizes an atom, there can be an emission characterized X-rays which is unique to each element[25]. The x-rays are unique to each element since the ejection of one election can allow another electron to move from a higher shell to the lower vacancy[25]. This process results in a release of energy that forms an x-ray that corresponds to a specific shell transition of energy[25].

In this work, EDS in conjunction with SEM was utilized to analyze the elemental composition of the samples to check the compositional changes.

2.4.4 RAMAN Spectroscopy

RAMAN spectroscopy is a non-destructive spectroscopic technique to determine vibrational modes of molecules. The instrument is composed of a light source, sample holder, monochromator, and a detector[26,27]. The light sources is a laser that provides a monochromatic beam. The sample holder is where the laser interacts with the material. Monochromator (wavelength sector) is the filter for the company Rayleigh scattering so that only the Raman-shifted light reaches the detector[26]. Lastly, the detector has two options. One is charge couples decide (CCD) or Photomultiplier tube (PMT) that converts the photons into an electrical signal so that a spectrum is produced[26,27].

The instrumentation is designed so that the inelastic scattering in relation to stokes and anti-stokes can be explored to get the chemical composition[26,27]. While the high energy laser injects photons into the sample to interact with the molecules there is photon scattering[26,27]. Scattering during this interaction can lead to elastic and inelastic. The elastic scattering, Rayleigh Scattering, results in the incident photon and the emitted photon to have almost identical energies[26,27]. The inelastic scattering, Raman scattering is when the incident photon undergoes a shift in the frequency due to an exchange in energy with the molecular bonds[26,27]. This shift gives information into the chemical makeup and bonds in the material.

Raman scattering is made up of two shifts, Stokes and Anti-stokes[26,27]. Stokes Raman scattering has a lower emitted photon frequency than the incident photon. For Stokes scattering to occur, the incident photon's energy is absorbed by the molecule[26,27]. Stokes scattering is more common than anti-stokes since the molecule starts at ground state for stokes[26,27]. Anti-stokes occurs when scattered photon is a higher frequency thane original photon[26,27]. This occurs when the incident light hits a molecules that is already in

an excited vibrational state so that the photon will "take" energy form the molecular bond and relaxes the molecule to a lower energy state[26,27].

For layers of 2D materials, such as bismuth selenide and bismuth oxyselenide, Raman spectroscopy is a quick nondestructive methos to confirm the percentage of specific phases and the crystalline quality. Peak position, intensity and width can provide information that is relevant to this study.

In this work, Raman Spectroscopy identified the vibration modes associated with the Bi-Se compounds and measured changes with the crystallinity with annealing. Samples with Ti could not be measured with this tool due to the metallic and reflective nature of Ti.

2.4.5 AFM

Atomic force microscopy (AFM) is a high-resolution surface characterization technique used to measure topography and nanoscale surface features. The components of an AFM device is a cantilever with a small sharp tip, a laser, and a photo detector[28]. The sharp tip at the end of the cantilever is deflected from the sample surface in accordance to Hooke's law[28]. Hooke's law describes the magnitude of the tip sample force proportional to the cantilever defelction[28]. There can be other interactions for repulsion to occur such as attraction with Van Der Waals forces, friction, adhesion, electrostatic interaction, and magnetic interaction[28]. In relation to the tip moving, the cantilever in turn also bends to indicate surface interaction. This bend is detected optically with a laser and photo detector[28].

With these components, the cantilever moves to create a raster scan as the detector notes the height of the probe. This process produces a three-dimensional surface topography map of the sample[28].

This interaction can happen with three imaging modes, contact mode, tapping mode, and non-contact mode. Contact mode is when the tip is rastered across the surface without the cantilever vibrating. This is good for rigid samples. As for tapping mode, the cantilever vibrates up and down at a resonance frequency, in other words, "taps" the surface lightly[28]. This reduces the lateral friction and damage compared to contact mode. Lastly, it is non-contact mode where the tip oscillates above the surface without touching it. This relies on van der Waals forces[28].

For this study AFM was used to characterize the surface morphology, roughness of the films, before and annealing. This gave insight into the structural changes associated with the annealing process, oxidation, and growth[28].

CHAPTER 3

EXPERIMENTAL METHODS AND GROWTH CONFIGURATIONS.

3.1 Overview of Experimental Design

This work is an investigation into the oxidation behavior of Bi2Se thin films under controlled conditions with a limited oxygen reservoir. The layered thin film structure was designed to help study this.

The general layer stack is composed of

- Substrate (Si or Sapphire)
- Bi-Se thin film (Bi_2Se_3 or Bi_2O_2Se)
- Oxide reservoir layer (HfO_2)
- Metal capping layer (Ti)

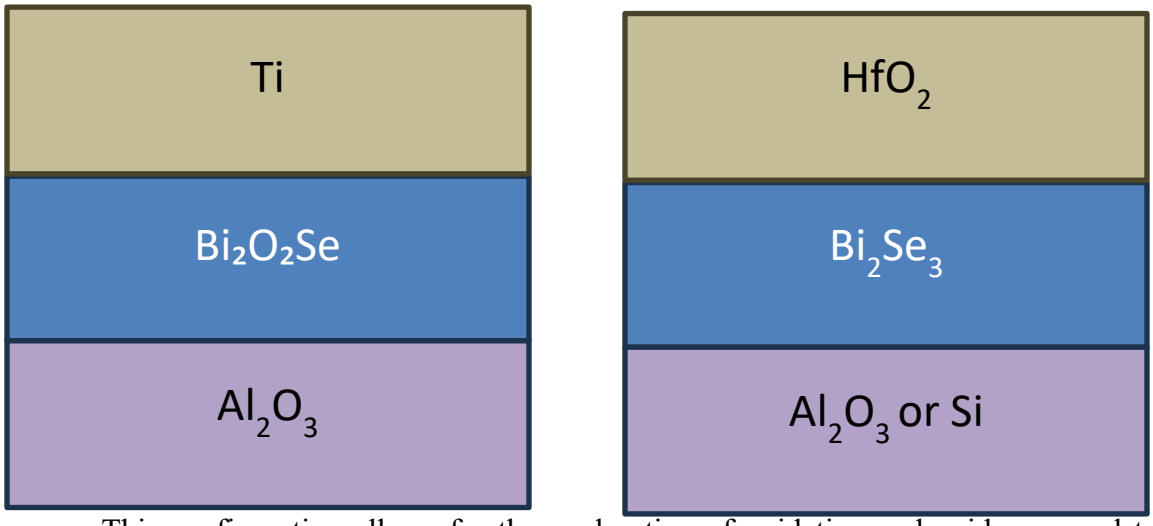

This configuration allows for the exploration of oxidation and oxide removal to understand the interactions. For instance, the stack of Si with Bi_2Se_3 and HfO_2 layer

provides understanding of the oxygen during thermal annealing. As for the Al2O3 with Bi_2O_2Se and Ti layers, overall oxidation dynamics can be explained.

The layer stack design is made with either a Si or Al2O3 substrate. On top of the Si and Al2O3 substrate there is a Bi_2Se_3 layer. As for Al2O3, there is a Bi_2O_2Se layer that is deposited by PLD. To have an oxygen reservoir for the Bi_2Se_3 to go through phase change to make Bi_2O_2Se.

3.2 Substrate Preparation

Prior to film deposition, all the substrates were cleaned with acetone, ethanol, and isopropyl alcohol (IPA). Each substrate was submerged and sonicated in these solvents for 5 minutes. Then they were then dried with Nitrogen gas. Afterwards the substrates were placed in an oxygen plasma cleaner.

Between the Al2O3 and the Silicon substates there are different exhibits of physical and chemical properties that influence thin film growth and oxidation behavior. Mechanical silicon substrates possess a native oxide layer compared to Al2O3. This can influence interface reactions, film adhesion, and stress development during the thermal process.

These differences within the substrates are expected to affect the oxidation behavior and phase formation of Bi_2O_2Se and Bi-Se thin films.

3.2.3 Substrate differences

The substrate is a critical choice for growth. Sapphire has a hexagonal corundum structure, and it has a lattice misfit of only 13% for Bi_2Se_3[29]. The large lattice mismatch

does not hinder the growth due to a lack of dangling bonds[29]. Without these dangling bonds, there is a great surface for the adatom migration, nucleation, and overall growth[29]. As for mechanical grade silicon, the structure is a diamond cubic with around a ~7.3% lattice mismatch[29]. Even with mechanical silicon, there is a native oxide layers with dangling bonds on the surface due to the reactivity of Si[29]. Thus there are some interesting effects interfacial disorder within the layers due to amorphous or a mixed phase interface with degrading crystallinity quality[29]. Also the Si with the native oxide creates an additional amorphous barrier[29].

This was even present for the growth of Bi_2O_2Se, where the growths preferred Al2O3 over Silicon.

3.3 CVD Setup

The chemical vapor deposition system used to deposit the Bi_2Se_3 is a single zone horizontal furnace with two flow meters to allow the flow of Argon and Oxygen into the 1in quartz tube. The setup was used for annealing and growth, where the tubes and interconnects were changed out each time for each respective task.

For growth, the substrates were put downstream around 430degreesC, and the powder Bi_2Se_3 precursor was placed upstream from the substrates in a ceramic sample boat around 630degreesC. There was a flow of 60sccm of Argon into the tube while a vacuum pump was running to maintain the pressure around 220mTorr during reaction. The best results for thin Bi_2Se_3 were when the material was less than 1mg of Bi_2Se_3 precursor and grown for only 3 minutes.

Annealing temperatures ranged from 150-550 for the single zone furnace. The samples were put directly in the center of the CVD to allow for the most heat during annealing. Also, there was a flow of 500sccm of Argon to ensure oxygen was not in the tube. This resulted in 1.02-1.04Torr of pressure during growth.

3.4 Capping layer depositions

HfO_2 was deposited through the ALD system in the ASU clean labs, and the Ti was deposited through a sputtering system in the ASU clean labs. The sample prep and work were done by my colleges.

CHAPTER 4

PRESENTS BI_2O_2SE OXIDATION AND ANNEALING RESULTS

4.1 Overview of Oxidation Experiments

The oxidation was carried out in the CVD furnace at various temperatures with the Bi_2Se_3 and the Bi_2O_2Se on Al2O3 and Si Substrates. This was to check the validity of the hypothesis to see if there can be successful scavenging and donation of oxygen through the capping layers to drive phase change in the bismuth selenium compounds.

to drive phase change in the bismuth selenium compounds.

The material configurations that were tested are outlined in the table below. Each configuration pairs a bismuth selenium thin film with either an oxygen reservoir or an oxygen scavenger capping layer.

Growth Method	Substrate	Material	Capping Layer
CVD	Silicon	Bi_2Se_3	HfO_2
PLD	Silicon	Bi_2Se_3	HfO_2
PLD	Al2O3	Bi_2O_2Se	Ti

Table 1. Material systems and capping layer configurations used in this study

For the oxygen reservoir configurations, the hypothesis was that HfO_2 or NiO would supply oxygen to the Bi_2Se_3 layer during thermal annealing so that the material can transition toward Bi_2O_2Se. As for the Ti capping layer on Bi_2O_2Se, the hypothesis was that Ti would act as an oxygen sink to pull oxygen out of the Bi_2O_2Se and allow a reduction back toward Bi_2Se_3.

4.2 Annealing Conditions

Thermal annealing was performed in a vacuum using a carefully regulated Argon atmosphere flowing at 500sccm. The annealing duration was 30 minutes for each sample. Earlier experiments with 2 hours of annealing were more than enough time, but 30 minutes gave comparable results and was more efficient for the number of samples being processed.

The annealing temperatures ranged from 150°C to 550°C depending on the material system. The temperatures at which the initial phase change was observed for each configuration are listed below.

Growth Method	**Substrate**	**Material**	**Capping Layer**	**Capping Thickness**	**Initial Phase Change Temp (C)**
CVD	Silicon	Bi_2Se_3	HfO_2	15 nm	550
PLD	Silicon	Bi_2Se_3	HfO_2	15 nm	550
PLD	Al2O3	Bi_2O_2Se	Ti	20 nm	150

Table 2. Onset temperatures for phase change observed across the material configurations.

Both HfO_2 capped systems showed phase change at 550°C regardless of whether the growth method of Bi_2Se_3 by CVD or PLD. The Ti capped system on Bi_2O_2Se showed phase change at a much lower temperature of 350°C. The difference of 200°C between the

reservoir and scavenger systems is a notable finding and will be discussed in relation to the characterization data below.

4.3 Oxygen Reservoir: CVD Bi_2Se_3 with HfO_2

The first material system that was characterized is the CVD grown Bi_2Se_3 on Silicon with a 15 nm HfO_2 capping layer deposited by ALD. This configuration was designed to test whether the HfO_2 can serve as a controlled oxygen source for the Bi_2Se_3 layer during annealing.

4.3.1 Raman and XRD Analysis

Raman spectroscopy was used to compare the as-deposited sample with the sample annealed at 550°C. Figure 5 shows the Raman spectra for the annealed and not annealed conditions.

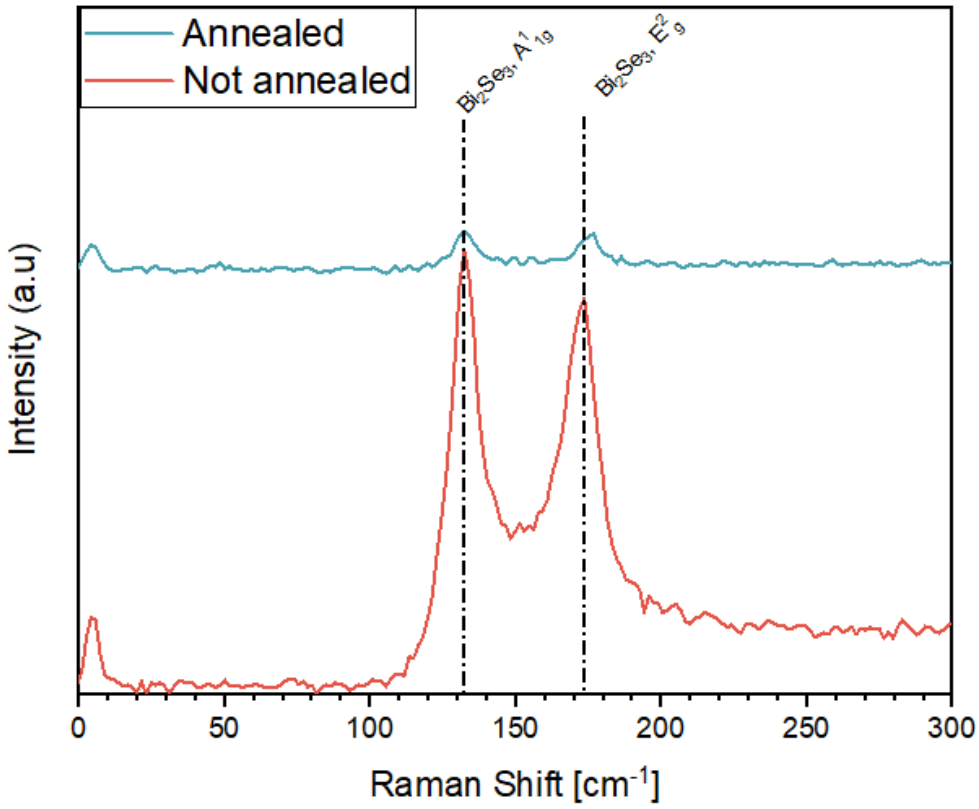

Figure 5. Raman spectra comparing the as-deposited (red) and annealed at 550°C (blue) CVD Bi_2Se_3 with HfO_2 capping layer on Si. The labeled peaks correspond to Bi_2Se_3 A^1_1g and E^2g vibrational modes.

In the as-deposited sample, the Raman spectrum shows the expected Bi_2Se_3 peaks at the A^1_1g and E^2g modes. After annealing at 550°C, a blue shift is observed in these peaks. Along with the shift, there are small peaks that arise between the main Bi_2Se_3 modes. The appearance of these intermediate peaks points to the formation of the Bi_2O_2Se phase in the material. The Bi_2Se_3 peaks are still present after annealing, which means the conversion is partial at this temperature and the material contains both phases.

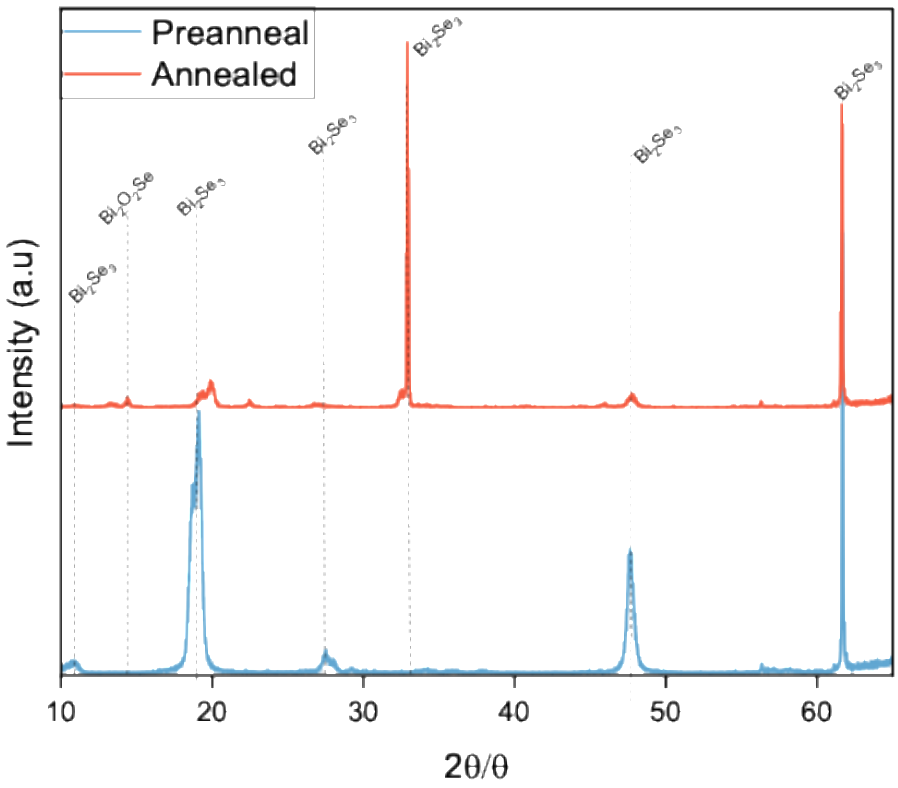

Figure 6. XRD graph comparing the as-deposited (red) and annealed at 550°C (blue) CVD Bi_2Se_3 with HfO_2 capping layer on Si. The labeled peaks correspond to the peaks with each respective crystal structure.

The XRD data for this sample also confirmed the formation of the Bi_2O_2Se phase. After annealing, the Bi_2Se_3 phase acquired a strong preferred orientation in the XRD pattern. The combination of the Raman and XRD results indicates that the HfO_2 capping layer was able to supply oxygen to the Bi_2Se_3 and drive a partial phase transformation toward Bi_2O_2Se at 550°C.

4.4 Oxygen Reservoir: PLD Bi_2Se_3 with HfO_2

The second configuration is the PLD grown Bi_2Se_3 on Silicon with the same 15 nm HfO_2 capping layer. This system was studied to see whether the same phase change behavior would occur when the Bi_2Se_3 is deposited by a different growth method.

4.4.1 XRD Analysis

XRD was performed on the PLD Bi_2Se_3 sample before and after annealing. Figure 7 shows the 2θ/θ scans for the pre-annealing and post-annealing conditions.

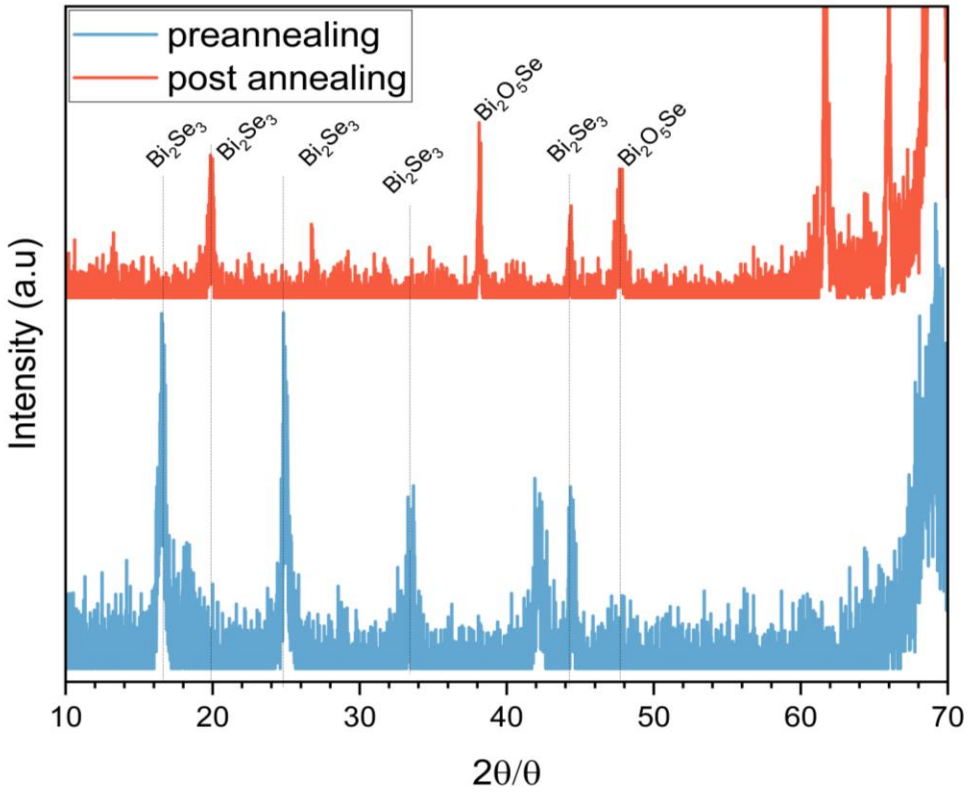

Figure 7. XRD 2θ/θ scans of PLD Bi_2Se_3 with HfO_2 on Si before annealing (blue) and after annealing at 550°C (red). Peak labels identify the Bi_2Se_3 and Bi_2O_5Se phases.

Before annealing, the XRD pattern shows multiple peaks that correspond to the Bi_2Se_3 phase. After annealing at 550°C, the XRD pattern changes. It is possible to observe the formation of the Bi_2O_5Se phase in the post-annealing scan. The remaining peaks in the annealed sample do not match the main peaks that were observed in the as-deposited condition. This indicates that the oxygen from the HfO_2 reservoir drove a more extensive transformation in the PLD sample compared to the CVD sample, where the Bi_2Se_3 peaks were still clearly present after annealing.

4.4.2 Raman Analysis

Raman spectroscopy was performed on the PLD Bi_2Se_3 sample at four conditions: no annealing, and after annealing at 350°C, 450°C, and 550°C. Figure 8 shows the Raman spectra at each temperature.

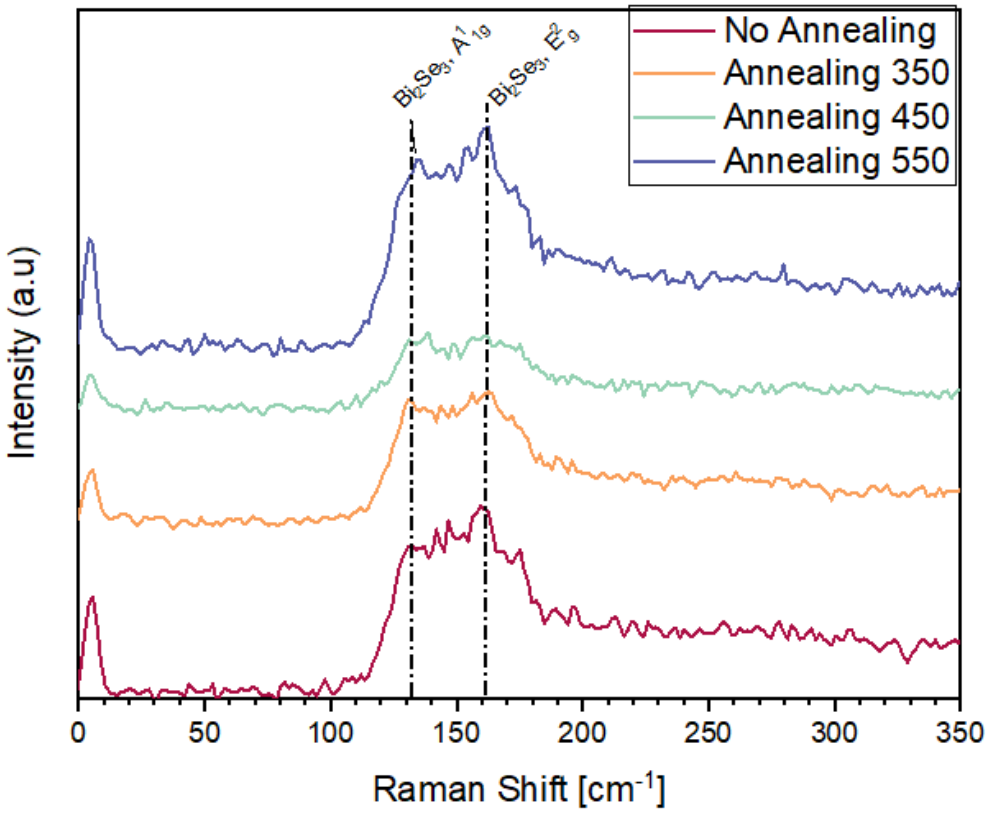

Figure 8. Raman spectra of PLD Bi_2Se_3 with HfO_2 on Si at four annealing conditions. The spectra are offset vertically for clarity. Dashed lines mark the Bi_2Se_3 A^1_1g and E^2g mode positions.

At the lower annealing temperatures of 350°C and 450°C, the Raman spectra do not show large changes from the as-deposited condition. The Bi_2Se_3 modes are still the dominant features. At 550°C, the spectrum changes more significantly with peak broadening and shifts in the Bi_2Se_3 mode positions. This temperature dependent behavior is consistent with the XRD finding that 550°C is the onset temperature for the phase transformation in this system.

The fact that both the CVD and PLD samples with HfO_2 capping layers showed phase change at the same temperature of 550°C is worth noting. Since the growth methods are different and would produce films with different microstructure and grain quality, the matching onset temperature suggests that the driving force for the oxidation is more dependent on the thermodynamic barrier of the oxygen transfer from HfO_2 rather than the quality of the starting Bi_2Se_3 film.

4.5 Oxygen Reservoir: Sputtered Bi_2Se_3 with NiO

The third oxygen reservoir configuration used sputtered Bi_2Se_3 on Silicon with a NiO capping layer. This was included to see whether a different metal oxide can also act as an oxygen reservoir for the phase change.

4.5.1 Raman Analysis

Raman spectroscopy was performed on the NiO capped sample before and after annealing. Figure 9 shows the comparison of the two spectra.

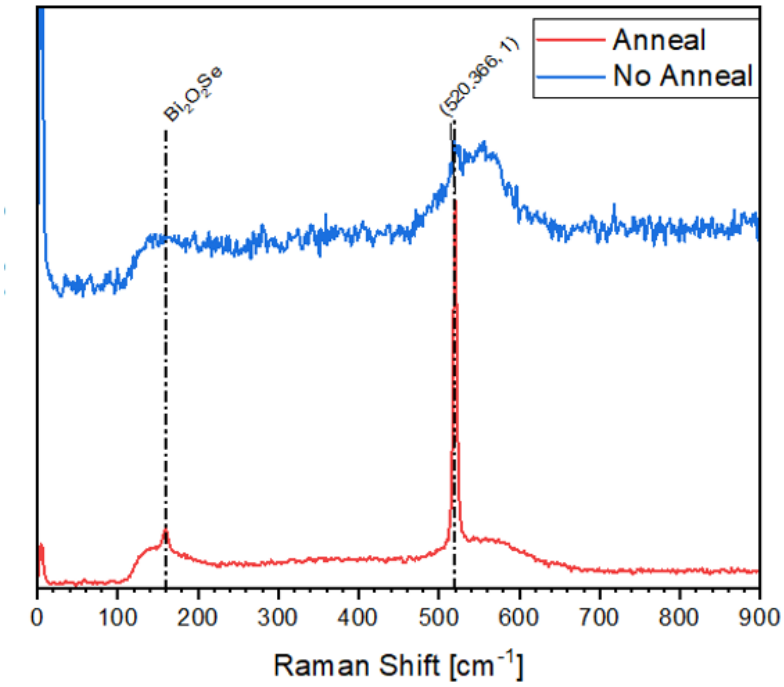

Figure 9. Raman spectra of sputtered Bi_2Se_3 with NiO capping on Si. The red spectrum is the as-deposited sample, and the blue spectrum is after annealing. Dashed lines mark the Bi_2O_2Se mode positions.

In the annealed sample, it is possible to observe the appearance of a Bi_2O_2Se Raman mode that was not present in the as-deposited spectrum. The Bi_2O_2Se mode near 520 cm^{-1} is visible in the annealed condition. This confirms that the NiO layer was able to donate oxygen to the Bi_2Se_3 layer and produce the Bi_2O_2Se phase, like the HfO_2 systems.

4.5.2 XRD Analysis

The XRD analysis of the NiO capped sample after annealing is shown in Figure 10.

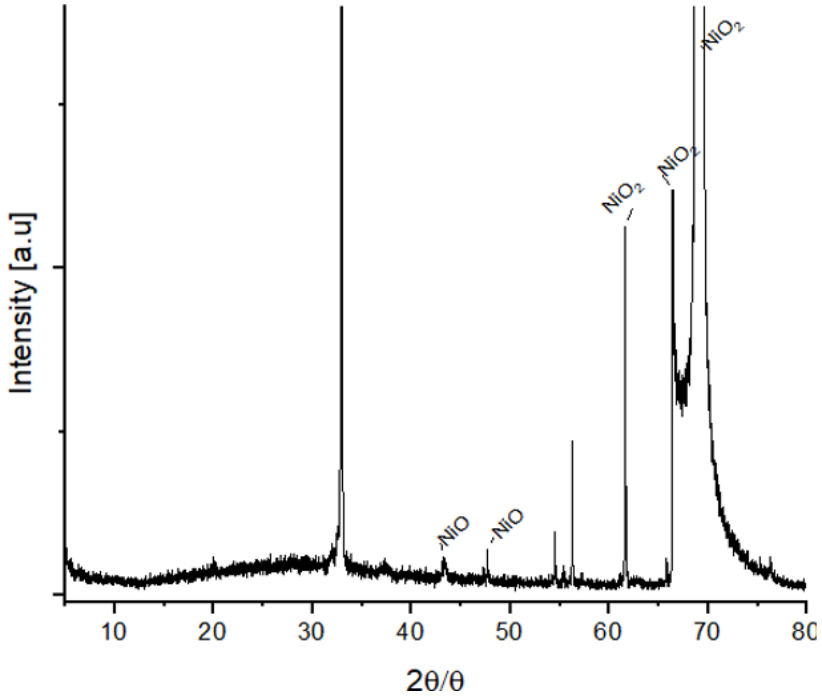

Figure 10. XRD 2θ/θ scan of sputtered Bi_2Se_3 with NiO on Si after annealing. The labeled peaks correspond to NiO, NiO_2, and Bi_2O_2Se phases.

The XRD pattern after annealing shows peaks corresponding to the NiO and NiO_2 phases from the capping layer. More importantly, the scan indicates the presence of a highly oriented out-of-plane Bi_2O_2Se phase. The strong preferred orientation of the Bi_2O_2Se in the XRD pattern along with the Raman confirmation makes this a clear case of oxygen transfer from the NiO reservoir into the film.

4.5.3 AFM Analysis

AFM was used to examine the surface morphology of the NiO capped sample before and after annealing. Figure 11 shows the surface topography maps for both conditions.

[Insert AFM images for sputtered Bi_2Se_3 / NiO — pre-anneal and annealed]

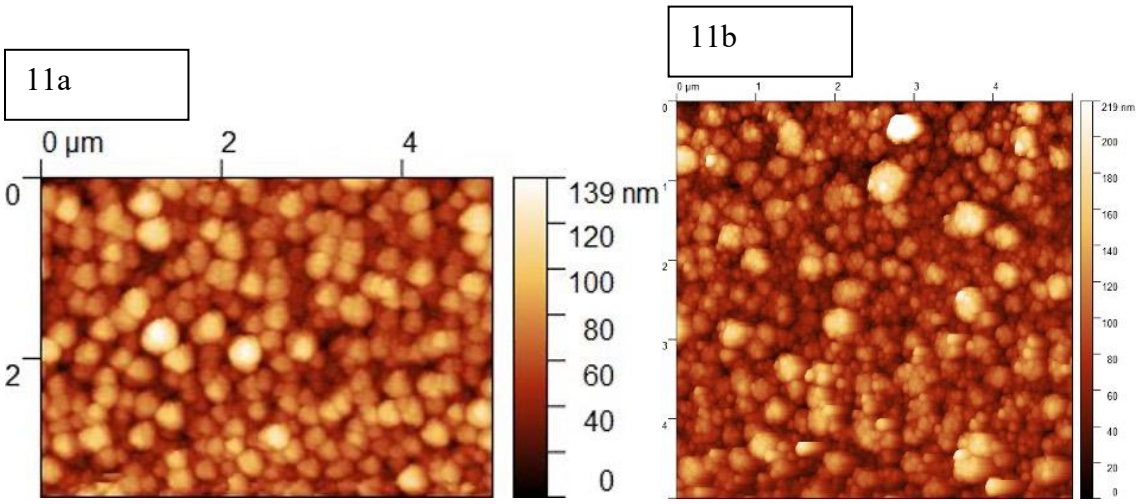

Figure 11. AFM topography maps of sputtered Bi_2Se_3 with NiO on Si. 10a: as-deposited (height range ~139 nm). 10b: after annealing (height range ~219 nm). Scan area is 4 × 4 µm.

The as-deposited sample shows a granular surface morphology with a height range of about 139 nm across the scan area. After annealing, the surface became coarser with larger agglomerated features and the height range increased to about 219 nm. The increase in surface roughness and the formation of larger surface features after annealing are consistent with the phase change and the oxygen incorporation into the film. The thermal treatment caused structural rearrangement at the surface, which is expected when the material undergoes a phase transformation.

4.5.4. SEM and EDS Analysis.

SEM and EDS were used to examine the cross-sectional structure and elemental composition of the NiO capped sample. Figure 12 shows the SEM and EDS results.

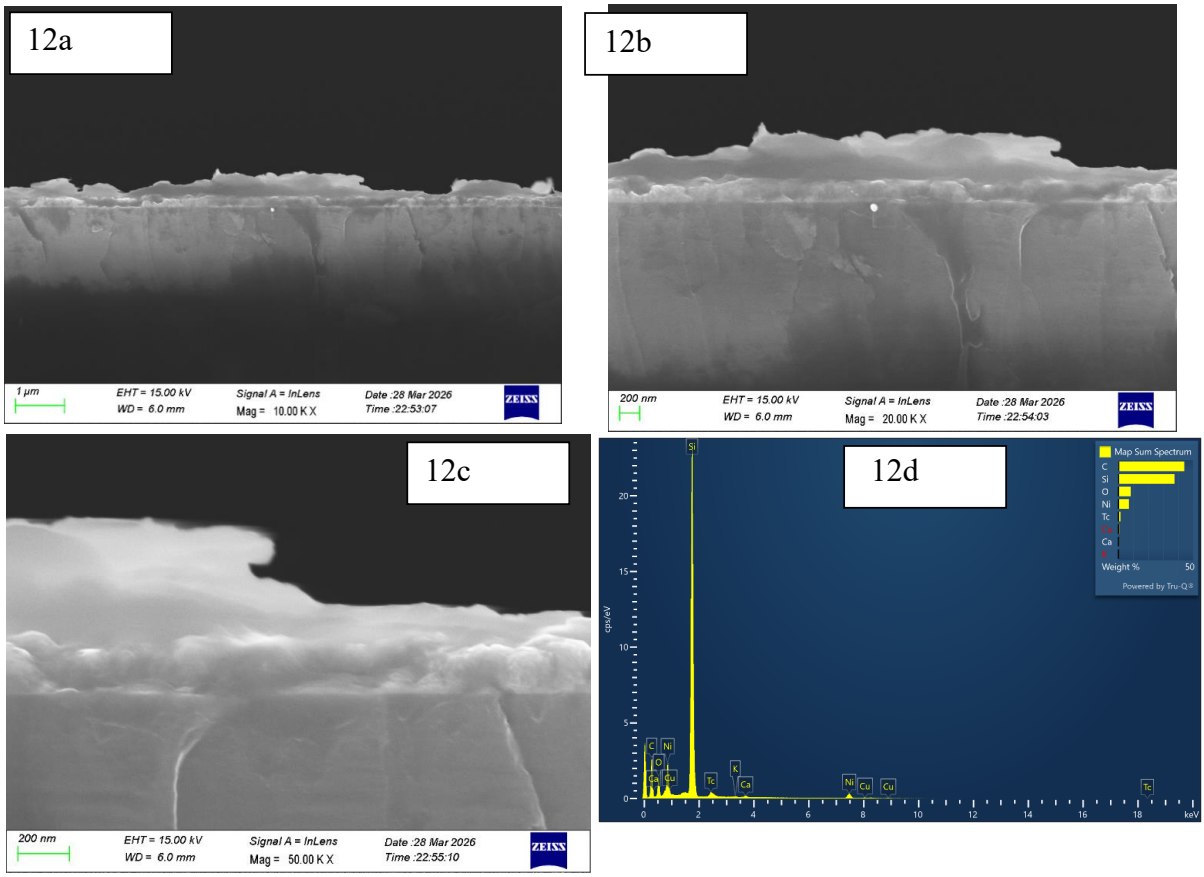

Figure 12.SEM cross-section images and EDS elemental maps of sputtered Bi_2Se_3 with NiO on Si.

The SEM cross-section shows the layered structure of the film stack. The EDS elemental mapping confirms the presence of Bi, Se, Ni, and O across the expected regions of the stack. The compositional distribution is consistent with the layer structure that was designed.

4.6 Oxygen Scavenger: PLD Bi_2O_2Se with Ti

The last configuration is the PLD grown Bi_2O_2Se on Al_2O_3 with a 20 nm Ti capping layer deposited by sputtering. Unlike the previous three systems, this configuration was designed to remove oxygen from the film rather than add it. The Ti layer was expected to act as an oxygen scavenger and pull oxygen out of the Bi_2O_2Se to drive a reduction toward Bi_2Se_3.

4.6.1 XRD Analysis

XRD was performed on the Ti capped Bi_2O_2Se at three conditions: pre-annealing, annealing at 150°C, and annealing at 350°C. Figure 6 shows the full range 2θ/θ scans and Figure 13b shows a zoomed in view of the region between 26° and 40°.

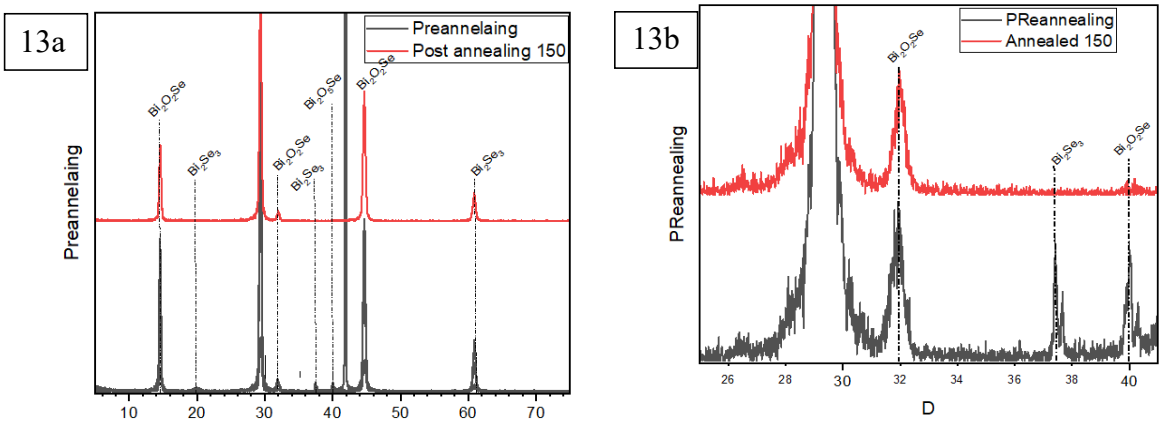

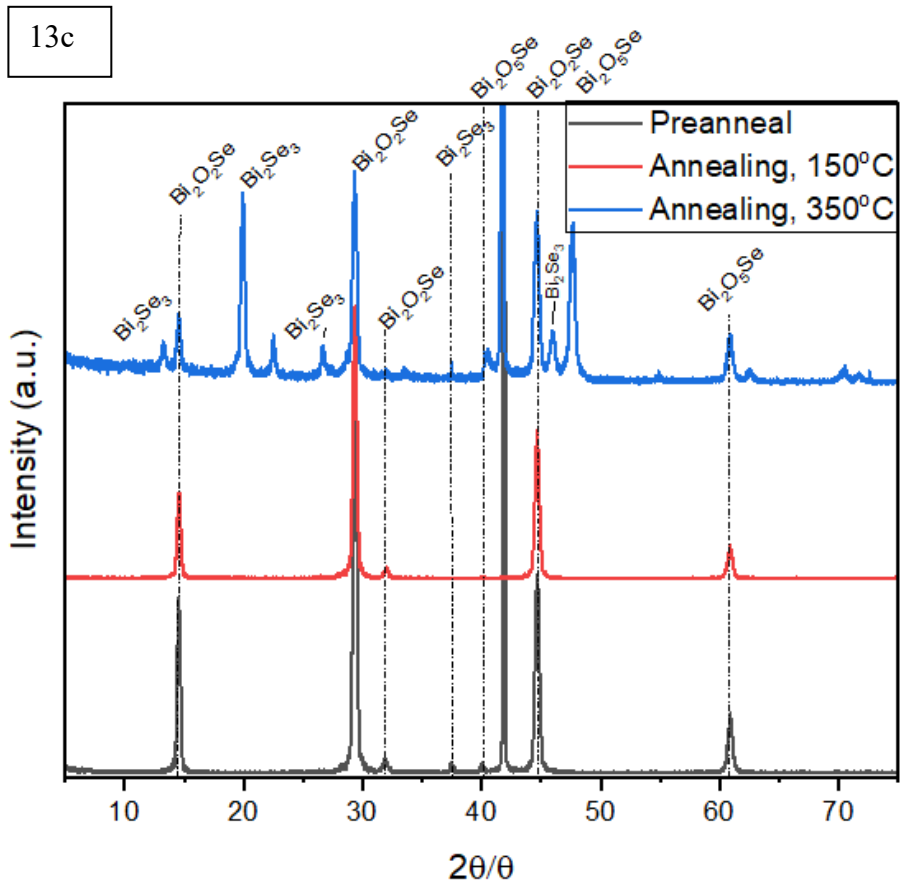

Figure 13. XRD 2θ/θ scans of PLD Bi_2O_2Se with Ti on Al_2O_3. Black: pre-annealing. Red: annealed at 150°C. Blue: annealed at 350°C. 13a. panel shows the full scan range and 13b. show the zoomed region from 26° to 40°. Peak labels identify Bi_2O_2Se, Bi_2Se_3, and Bi_2O_2Se phases. 13c shows a full panel at 350°C

The pre-annealing XRD pattern shows clear Bi_2O_2Se peaks along with some Bi_2Se_3 peaks. The presence of Bi_2Se_3 in the as-deposited sample indicates that the starting material already had mixed phases before any thermal treatment.

After annealing at 150°C, the XRD pattern shows an improvement in the crystallinity of the Bi_2O_2Se peaks. The peaks become sharper and more defined compared to the pre-annealing condition. However, at this temperature the transition to Bi_2Se_3 is not clear from the XRD data alone. The low temperature anneal appears to have improved the crystal quality of the existing phases without driving a significant phase change.

At 350°C, the XRD data shows more change. It is possible to observe peaks corresponding to the Bi_2Se_3 phase becoming stronger in the pattern. The material at this temperature has mixed phases with both Bi_2O_2Se and Bi_2Se_3 present. This is consistent with the Ti layer scavenging oxygen from the Bi_2O_2Se and allowing some of the material to reduce toward Bi_2Se_3. The onset of this change at 350°C is about 200°C lower than the onset temperature for the HfO_2 oxygen reservoir systems.

4.6.2 Raman Analysis

Raman spectroscopy was performed on the Ti capped sample at multiple conditions including no annealing, annealed, and an annealed surface spot measurement. Figure X shows the Raman spectra.

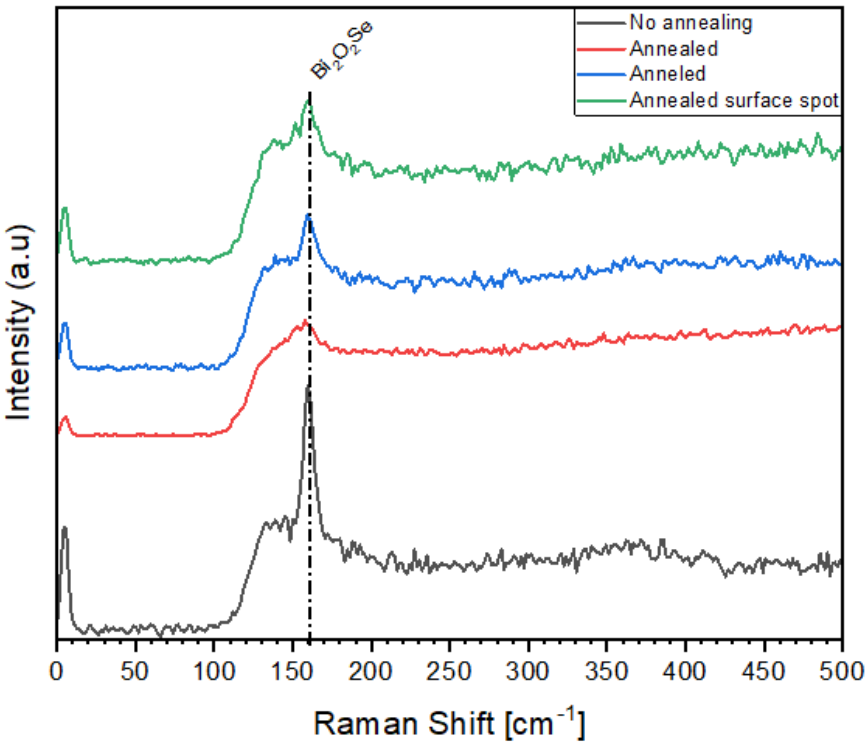

Figure 14. Raman spectra of PLD Bi_2O_2Se with Ti on Al_2O_3 at different conditions. The Bi_2O_2Se mode position is marked with a dashed line.

The Raman data for the Ti capped samples was limited due to the metallic and reflective nature of the Ti surface layer. The Ti layer makes it difficult for the laser to penetrate through to the Bi_2O_2Se film underneath. In the spectra that were collected, the Bi_2O_2Se mode is still visible, which indicates that the phase change is not complete even after annealing. The material retains some Bi_2O_2Se character while also showing evidence

of Bi_2Se_3 formation in the XRD, confirming the mixed phase nature of the annealed material.

4.6.3 AFM Analysis

AFM was used to characterize the surface morphology of the Ti capped Bi_2O_2Se before and after annealing. Figure X shows the topography maps.

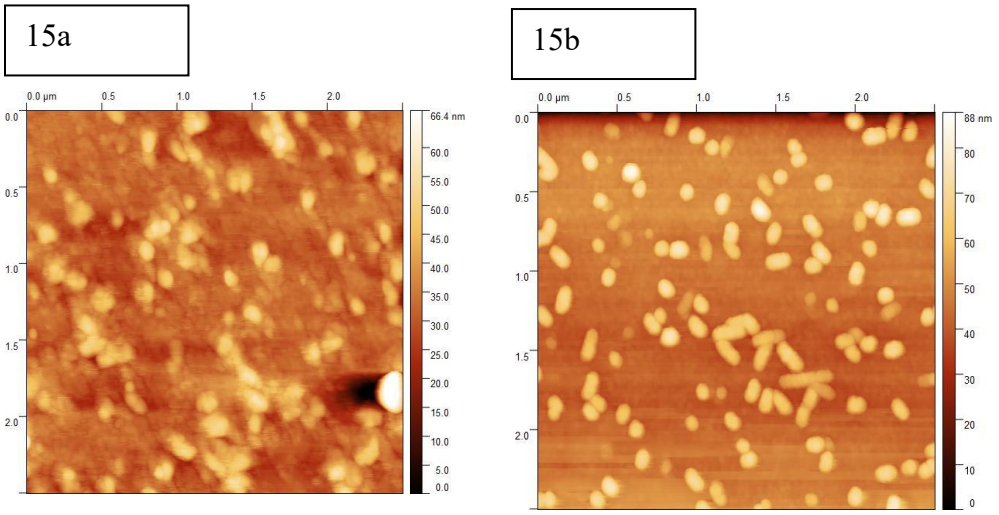

Figure 15. AFM topography maps of PLD Bi_2O_2Se with Ti on Al_2O_3. 15a: as-deposited (height range ~66.4 nm, scan area 2.6 × 2.6 µm). 15b: after annealing (height range ~88 nm, scan area 2 × 2 µm).

The as-deposited sample has a surface with granular island features and a height range of about 66.4 nm. After annealing, the surface changes to show fewer but larger features with a smoother overall appearance. The height range increased to about 88 nm. The change in surface morphology from many small islands to fewer larger features suggests that the annealing caused grain growth and surface reconstruction. The smoother character of the annealed surface compared to the NiO reservoir system is possibly related

to the different substrate and the different direction of the oxygen transport. In the NiO system, oxygen was being added to the film, while in this system oxygen was being removed.

4.7 Comparison Across Systems

Across the four material configurations, the characterization data confirms that both the oxygen reservoir and oxygen scavenger approaches can drive phase change in bismuth selenium compounds. The HfO_2 and NiO capping layers successfully donated oxygen to Bi_2Se_3 to produce Bi_2O_2Se, while the Ti capping layer pulled oxygen from Bi_2O_2Se to produce Bi_2Se_3.

One of the main findings from the temperature data is the difference in onset temperatures between the two directions of phase change. The oxygen reservoir systems with HfO_2 required 550°C before the phase change was detectable in XRD and Raman. As for the Ti oxygen scavenger system, phase change was already apparent at 350°C. This 200°C gap suggests that it takes more energy to break the oxygen out of HfO_2 and incorporate it into the Bi_2Se_3 lattice than it does for Ti to extract oxygen from Bi_2O_2Se. In other words, the barrier for oxygen donation is higher than the barrier for oxygen removal in these material systems.

The fact that the CVD and PLD grown Bi_2Se_3 films both showed onset at 550°C with the HfO_2 layer adds to this point. If the film microstructure or grain boundaries were the main factor controlling the onset temperature, the two growth methods would likely show different temperatures due to their different film qualities. Since they did not, the

thermodynamic barrier of the capping layer reaction appears to be the more important factor.

The NiO system provides further evidence that the reservoir concept works with different metal oxide materials. The appearance of Bi_2O_2Se modes in Raman and the highly oriented Bi_2O_2Se phase in XRD after annealing show that NiO is a viable alternative to HfO_2 as an oxygen source. The AFM data from both the NiO and Ti systems shows that the surface morphology changes with the phase transformation, which is expected given that the crystal structure is changing.

Looking at the overall results, the capping layers after annealing would have changed composition as well. The HfO_2 layer would become HfO_{2-x} as it loses oxygen to the film. The NiO layer would similarly become NiO_x. As for the Ti layer, it would oxidize to TiO_x as it picks up oxygen from the Bi_2O_2Se. These compositional changes in the capping layers are part of the oxygen transport pathway and are consistent with the mechanism that was proposed in Chapter 1.

CHAPTER 5

SUMMARIZES KEY FINDINGS AND OUTLINES FUTURE DIRECTIONS

5.1 summary of results

This work studied the oxidation of bismuth selenide and bismuth oxyselenide thin films with controlled capping layers. The idea was to use metal oxide layers as limited oxygen reservoirs and metal layers as oxygen scavengers to drive phase change between Bi_2Se_3 and Bi_2O_2Se. Layered thin film stacks were designed with HfO_2 and NiO as oxygen reservoirs on Bi_2Se_3, and Ti as an oxygen scavenger on Bi_2O_2Se. The annealed samples ran at various temperatures under vacuum with Argon flow to observe the conditions needed for the phase transformation.

Four material configurations were highlighted in the study. CVD grown Bi_2Se_3 on Silicon with a 15 nm HfO_2 capping layer, PLD grown Bi_2Se_3 on Silicon with the same 15 nm HfO_2 layer, sputtered Bi_2Se_3 on Silicon with a NiO capping layer, and PLD grown Bi_2O_2Se on Al_2O_3 with a 20 nm Ti capping layer.

For both of the HfO_2 capped Bi_2Se_3 systems, the initial phase change was observed at 550°C. The CVD and PLD grown films showed the same onset temperature even though the two growth methods produce films with different microstructure and grain quality. Since both hit 550°C, the onset temperature seems to depend more on the energy needed for HfO_2 to release oxygen into the Bi_2Se_3 rather than the film quality itself. The HfO_2 worked as the limited oxygen source that was intended, and the Bi_2Se_3 was able to pick up oxygen and move toward the Bi_2O_2Se phase.

The NiO capping layer on sputtered Bi_2Se_3 also showed that a different metal oxide can serve the same reservoir role. After annealing, Bi_2O_2Se modes appeared in Raman and the XRD showed a highly oriented out-of-plane Bi_2O_2Se phase. This adds to the evidence that the oxygen reservoir concept is not limited to just HfO_2.

As for the Ti capped Bi_2O_2Se on Al_2O_3, the phase change showed up at 350°C, which is 200°C lower than the HfO_2 systems. The Ti acted as a scavenger and pulled oxygen out of the Bi_2O_2Se. At 150°C there was some crystallinity improvement in the XRD but no clear Bi_2Se_3 formation. At 350°C the Bi_2Se_3 peaks started to appear alongside the Bi_2O_2Se peaks, so the material was in a mixed phase state. The 200°C difference between the reservoir and scavenger onset temperatures is notable. It takes less energy for Ti to pull oxygen out of Bi_2O_2Se than it does for HfO_2 to push oxygen into Bi_2Se_3. The barrier for removing oxygen is lower than the barrier for adding it in these compounds.

The characterization tools used to confirm these findings each played a different role. XRD was the main tool for identifying the phases before and after annealing. Raman gave a nondestructive way to check for phase change through the vibrational modes of Bi_2Se_3 and Bi_2O_2Se. It should be noted that the Ti capped samples could not be measured with Raman due to the reflective nature of the Ti surface. AFM was used to look at the surface morphology changes. For the NiO system, the surface went from a granular morphology with a height range of about 139 nm to coarser features at about 219 nm after annealing. As for the Ti system, the surface went from granular islands at about 66.4 nm to smoother and larger features at about 88 nm.

The choice of substrate also mattered. Silicon was used for its relevance to semiconductor processing, but Bi_2O_2Se did not deposit well directly onto Silicon. Due to this, Al_2O_3 was used as the substrate for the Bi_2O_2Se samples since it has a better lattice match. The differences in substrate properties like thermal stability and interface chemistry are expected to have some influence on the oxidation behavior across the different stacks.

After annealing, the capping layers would have changed composition as well. The HfO_2 would lose oxygen and become HfO_{2-x}, the NiO would similarly become NiO_x, and the Ti would oxidize to TiO_x. These changes in the capping layers are part of the oxygen transport pathway and are consistent with the mechanism that was laid out in Chapter 1.

With all of the configurations taken together, the main takeaway is that controlled phase transformation between Bi_2Se_3 and Bi_2O_2Se can be done through the engineering of these capping layers. The oxygen can be moved in either direction depending on whether the capping material is an oxide that wants to give up oxygen or a metal that wants to take it.

5.2 Future Work

There are several directions that can build on this work. The first is to study the interfaces between the capping layer and the thin film more closely. Understanding how the capping layer interacts with the bismuth selenium film at the atomic level would give more information about the diffusion pathways for the oxygen transport. Cross-sectional TEM would be useful for this since it can resolve the interface structure at a finer scale than what SEM can provide.

Another direction is to see if the process can be made reversible. In this work, the phase change was driven in one direction for each configuration. It would be useful to know if a sample that was converted from Bi_2Se_3 to Bi_2O_2Se through an oxygen reservoir can then be converted back by applying an oxygen scavenger layer and annealing again. If the process is reversible, it opens up possibilities for switchable material properties.

There is also the question of capping layer thickness. This work used 15 nm of HfO_2 and 20 nm of Ti. Changing the thickness of the capping layer would change the amount of oxygen available in the reservoir or the capacity of the scavenger. Studying how the thickness affects the degree of phase conversion and the onset temperature would be valuable for tuning the process.

Lastly, the fabrication of devices using these capping layers is a goal for this work moving forward. If the phase change can be controlled well enough, it could be used for device applications where switching between Bi_2Se_3 and Bi_2O_2Se gives different electronic properties. Building a simple device structure on these materials would be the next step toward showing that this approach has practical value beyond the material characterization level.

REFERENCES

(1) *Controllable and fast growth of high-quality atomically thin and atomically flat Bi2O2Se films | Applied Physics Letters | AIP Publishing*. https://pubs.aip.org/aip/apl/article-abstract/125/17/171903/3318233/Controllable-and-fast-growth-of-high-quality?redirectedFrom=fulltext (accessed 2026-03-24).

(2) Novoselov, K. S.; Geim, A. K.; Morozov, S. V.; Jiang, D.; Zhang, Y.; Dubonos, S. V.; Grigorieva, I. V.; Firsov, A. A. Electric Field Effect in Atomically Thin Carbon Films. *Science* **2004**, *306* (5696), 666–669. https://doi.org/10.1126/science.1102896.

(3) Novoselov, K. S.; Mishchenko, A.; Carvalho, A.; Castro Neto, A. H. 2D Materials and van Der Waals Heterostructures. *Science* **2016**, *353* (6298), aac9439. https://doi.org/10.1126/science.aac9439.

(4) Ren, W.; Bøggild, P.; Redwing, J.; Novoselov, K. S.; Sun, L.; Qi, Y.; Jia, K.; Liu, Z.; Burton, O.; Alexander-Webber, J.; Hofmann, S.; Cao, Y.; Long, Y.; Yang, Q.-H.; Li, D.; Choi, S. H.; Kim, K. K.; Lee, Y. H.; Li, M.; Huang, Q.; Gogotsi, Y.; Clark, N.; Carl, A.; Gorbachev, R.; Olsen, T.; Rosen, J.; Thygesen, K. S.; Efetov, D. K.; Jessen, B. S.; Yankowitz, M.; Barrier, J.; Kumar, R. K.; Koppens, F. H.; Deng, H.; Li, X.; Dai, S.; Basov, D. N.; Wang, X.; Das, S.; Duan, X.; Yu, Z.; Borsch, M.; Ferrari, A. C.; Huber, R.; Kira, M.; Xia, F.; Wang, X.; Wu, Z.-S.; Feng, X.; Simon, P.; Cheng, H.-M.; Liu, B.; Xie, Y.; Jin, W.; Nair, R. R.; Xu, Y.; Zhang, Q.; Katiyar, A. K.; Ahn, J.-H.; Aharonovich, I.; Hersam, M. C.; Roche, S.; Hua, Q.; Shen, G.; Ren, T.; Zhang, H.-B.; Koo, C. M.; Koratkar, N.; Pellegrini, V.; Young, R. J.; Qu, B.; Lemme, M.; Pollard, A. J. The 2D Materials Roadmap. *2D Mater.* **2026**, *13* (2), 021501. https://doi.org/10.1088/2053-1583/ae2b82.

(5) Lee, B. H.; Oh, J.; Tseng, H. H.; Jammy, R.; Huff, H. Gate Stack Technology for Nanoscale Devices. *Mater. Today* **2006**, *9* (6), 32–40. https://doi.org/10.1016/S1369-7021(06)71541-3.

(6) Kelly, M. J. *Low-Dimensional Semiconductors: Materials, Physics, Technology, Devices*; Clarendon Press, 1995.

(7) Li, T.; Peng, H. 2D Bi2O2Se: An Emerging Material Platform for the Next-Generation Electronic Industry. *Acc. Mater. Res.* **2021**, *2* (9), 842–853. https://doi.org/10.1021/accountsmr.1c00130.

(8) Sagar, R. U. R.; Khan, U.; Galluzzi, M.; Aslam, S.; Nairan, A.; Anwar, T.; Ahmad, W.; Zhang, M.; Liang, T. Transfer-Free Growth of Bi2O2Se on Silicon Dioxide via Chemical Vapor Deposition. *ACS Appl. Electron. Mater.* **2020**, *2* (7), 2123–2131. https://doi.org/10.1021/acsaelm.0c00344.

(9) Ding, X.; Li, M.; Chen, P.; Zhao, Y.; Zhao, M.; Leng, H.; Wang, Y.; Ali, S.; Raziq, F.; Wu, X.; Xiao, H.; Zu, X.; Wang, Q.; Vinu, A.; Yi, J.; Qiao, L. Bi2O2Se: A Rising Star for Semiconductor Devices. *Matter* **2022**, *5* (12), 4274–4314. https://doi.org/10.1016/j.matt.2022.11.005.

(10) Huang, C.; Yu, H. Two-Dimensional Bi2O2Se with High Mobility for High-Performance Polymer Solar Cells. *ACS Appl. Mater. Interfaces* **2020**, *12* (17), 19643–19654. https://doi.org/10.1021/acsami.0c01364.

(11) Larsson, K. *Chemical Vapour Deposition: Growth Processes on an Atomic Level*; IOP Publishing, 2022.

(12) Wasa, K.; Hayakawa, S. *Handbook of Sputter Deposition Technology: Principles, Technology, and Applications*; Materials science and process technology series; Noyes Publications: Park Ridge, N.J., U.S.A, 1992.

(13) Atkins, P.; Paula, J. D.; Keeler, J. *Atkins' Physical Chemistry*, 12th ed.; Oxford University Press, 2022. https://doi.org/10.1093/hesc/9780198847816.001.0001.

(14) *Structure and Dynamics of Surfaces II: Phenomena, Models, and Methods (Topics in Current Physics #43) (Paperback) | Third Place Books*. https://www.thirdplacebooks.com/book/9783642465932 (accessed 2026-03-30).

(15) Chrisey, D. B.; Hubler, G. K. *Pulsed Laser Deposition of Thin Films*; 2003.

(16) Liu, F.; Liu, M.; Liu, A.; Yang, C.; Chen, C.; Zhang, C.; Bi, D.; Man, B. The Effect of Temperature on Bi2Se3 Nanostructures Synthesized via Chemical Vapor Deposition. *J. Mater. Sci. Mater. Electron.* **2015**, *26* (6), 3881–3886. https://doi.org/10.1007/s10854-015-2915-5.

(17) *Transfer-Free Growth of Bi2O2Se on Silicon Dioxide via Chemical Vapor Deposition | ACS Applied Electronic Materials*. https://pubs.acs.org/doi/10.1021/acsaelm.0c00344 (accessed 2026-03-30).

(18) Lee, D. Recent Advances in Chemical Vapor Deposition of Bi2O2Se and Its Applications in Energy-Efficient Electronics. *Int. J. Energy Res.* **2025**, *2025* (1), 1612449. https://doi.org/10.1155/er/1612449.

(19) Johnson, R. W.; Hultqvist, A.; Bent, S. F. A Brief Review of Atomic Layer Deposition: From Fundamentals to Applications. *Mater. Today* **2014**, *17* (5), 236–246. https://doi.org/10.1016/j.mattod.2014.04.026.

(20) Harrington, G. F.; Santiso, J. Back-to-Basics Tutorial: X-Ray Diffraction of Thin Films. *J. Electroceramics* **2021**, *47* (4), 141–163. https://doi.org/10.1007/s10832-021-00263-6.

(21) *SmartLab*. https://rigaku.com/products/x-ray-diffraction-and-scattering/xrd/smartlab (accessed 2026-03-30).

(22) Zhou, W.; Apkarian, R.; Wang, Z. L.; Joy, D. Fundamentals of Scanning Electron Microscopy (SEM). In *Scanning Microscopy for Nanotechnology: Techniques and Applications*; Zhou, W., Wang, Z. L., Eds.; Springer: New York, NY, 2007; pp 1–40. https://doi.org/10.1007/978-0-387-39620-0_1.

(23) Vernon-Parry, K. D. Scanning Electron Microscopy: An Introduction. *III-Vs Rev.* **2000**, *13* (4), 40–44. https://doi.org/10.1016/S0961-1290(00)80006-X.

(24) *What is Scanning Electron Microscopy?* https://www.jeolusa.com/RESOURCES/Electron-Optics/Scanning-Electron-Microscopy-Basics (accessed 2026-03-30).

(25) *Energy-Dispersive X-ray Spectroscopy (EDS) - Chemistry LibreTexts*. https://chem.libretexts.org/Courses/Franklin_and_Marshall_College/Introduction_to_Materials_Characterization__CHM_412_Collaborative_Text/Spectroscopy/Energy-Dispersive_X-ray_Spectroscopy_(EDS) (accessed 2026-03-30).

(26) *4.3: Raman Spectroscopy*. Chemistry LibreTexts. https://chem.libretexts.org/Bookshelves/Analytical_Chemistry/Physical_Methods_in_Chemistry_and_Nano_Science_(Barron)/04%3A_Chemical_Speciation/4.03%3A_Raman_Spectroscopy (accessed 2026-03-30).

(27) *Guide to Raman Spectroscopy*. https://www.bruker.com/en/products-and-solutions/raman-spectroscopy/raman-basics/what-is-raman-spectroscopy.html (accessed 2026-03-30).

(28) Jagtap, R. N.; Ambre, A. H. Overview Literature on Atomic Force Microscopy (AFM): Basics and Its Important Applications for Polymer Characterization. *INDIAN J ENG MATER SCI* **2006**.

(29) Lee, Y. F.; Punugupati, S.; Wu, F.; Jin, Z.; Narayan, J.; Schwartz, J. Evidence for Topological Surface States in Epitaxial Bi2Se3 Thin Film Grown by Pulsed Laser Deposition through Magneto-Transport Measurements. *Curr. Opin. Solid State Mater. Sci.* **2014**, *18* (5), 279–285. https://doi.org/10.1016/j.cossms.2014.07.001.

(30) Zhakhovsky, V. V.; Kryukov, A. P.; Levashov, V. Yu.; Shishkova, I. N.; Anisimov, S. I. Mass and Heat Transfer between Evaporation and Condensation Surfaces: Atomistic Simulation and Solution of Boltzmann Kinetic Equation. *Proc.*

Natl. Acad. Sci. U. S. A. **2019**, *116* (37), 18209–18217. https://doi.org/10.1073/pnas.1714503115.

(31) Sputter Processing. In *Handbook of Thin Film Deposition*; William Andrew Publishing, 2018; pp 195–230. https://doi.org/10.1016/B978-0-12-812311-9.00007-4.